Letters in Applied NanoBioScience
Open-Access Journal (ISSN: 2284-6808)

Article
Volume 13, Issue 4, 2024, 199
https://doi.org/10.33263/LIANBS134.199

Polypharmacological and Computational Approaches to Establish HDAC Inhibitors in the Treatment of Alzheimer

Pallavi Pandey [1], Prinsa [2], Vikash Jakhmola [1], Mohammad Asif [3], Supriyo Saha [1,*]

[1] Department of Pharmaceutical Chemistry, Uttaranchal Institute of Pharmaceutical Sciences, Uttaranchal University, Dehradun-248007, Uttarakhand, India
[2] Siddhartha Institute of Pharmacy, Sahastradhara Road Near IT-Park Dehradun 248001, India
[3] Department of Pharmaceutical Chemistry, Era College of Pharmacy, Era University, Lucknow, 226003, Uttar Pradesh, India
* Correspondence: supriyo9@gmail.com (S.S.);

Scopus Author ID55844991200
Received: 25.04.2023; Accepted: 29.05.2023; Published: 28.08.2024

Abstract: Alzheimer's is a progressive cognitive condition with significant loss of neuronal functions, formation of amyloid plaque, and neurofibrillary tangles. Gamma secretase, acetylcholinesterase (AChE), butyrylcholinesterase (BuChE), and GSK-3beta enzymes regulated the progression of Alzheimer's disease. HDAC6 enzyme also improved the axonal activity linked to Alzheimer's disease. In this manuscript, we repurposed the role of HDAC inhibitors [$HDACi_{(s)}$] towards the treatment of Alzheimer's disease by inhibiting gamma-secretase (6LQG), AChE (7AIT), BuChE (6QAE), and GSK-3beta (3GB2) enzymes. Here, we considered 60 HDACI and then filtered out 16 molecules using SWISS-ADME parameters. Docking score of Analog 45 and Analog 57 against 6LQG, 7AIT, 6QAE and 3GB2 were (-) 8.1 kcal/mol, (-) 10.5 kcal/mol, (-) 9.1 kcal/mol, (-) 7.3 kcal/mol and (-) 8.2 kcal/mol, (-) 11.5 kcal/mol, (-) 9.5 kcal/mol, (-) 8.0 kcal/mol respectively; whereas Rivastigmine showed docking score of (-) 5.3 kcal/mol, (-) 8.0 kcal/mol, (-) 7.2 kcal/mol, (-) 6.1 kcal/mol. Based on docking score, we selected (E)-N-(2-amino-4-fluorophenyl)-3-(1-cinnamyl-1H-1,2,3-triazol-4-yl)acrylamide (Analog 45), N-methyl-4-((3-(pyrrolidin-1-ylmethyl)-1H-indol-1-yl)methyl)benzamide (Analog 57) and Rivastigmine for further studies. Then, we performed OSIRIS-MOLINPIRATION profiling to observe the most effective and low-toxic molecule. Analog 57 passed the criteria. Finally, we performed FMO and EPS analyses using (B3LYP) 6-311G+(d,p) to observe the electronic nature of the molecule. HOMO orbital localized on the indole nucleus and LUMO orbital localized on N-methyl benzamide group.EPS analysis data showed that nitrogen atoms of pyrrolidine and indole [3-[(pyrrolidin-1-yl)methyl]-1*H*-indole of this nucleus] and also O=C-N of benzamide nucleus were feasible for the electrophilic attack. In the same manner, benzene of the indole ring and terminal methyl group of benzamide were suitable for nucleophilic attack. Finally, we stated that N-methyl-4-((3-(pyrrolidin-1-ylmethyl)-1H-indol-1-yl)methyl) benzamide is the best molecule repurposed for the management of Alzheimer's.

Keywords: Polypharmacology; HDAC inhibitor; Alzheimer's; molecular docking; OSIRIS-MOLINSPIRATION; FMO analysis; ESP analysis.

1. Introduction

Alzheimer's disease (AD) is an age-related cognitive condition that is associated with a significant decline in memory and learning abilities due to the loss of neuronal functions. Among the most common types of dementia is AD. An unhealthy type of AD results from the

sequential cleavage of amyloid precursor protein (APP) by β-secretase and γ-secretase. The causes of AD include neuron death, insoluble amyloid plaque, and neurofibrillary tangles (NFTs). According to the currently accepted theory described as the "Amyloid cascade hypothesis," an excessive accumulation of β -amyloid triggers a complex chain of neuronal death, resulting in AD onset [1]. Extracellular aggregation of A-peptides as senile plaques is a typical neuropathological indicator of AD. In India, more than 50 lakh people, and worldwide, nearly 50 million persons suffer from Alzheimer's disease. Dementia is not only a symptom of Alzheimer's; persons also suffer from impaired cognitive behavior and memory, mood swings, and confusion during identification of geographical position. The hippocampus is associated with learning and cognitive behavior, and in Alzheimer's, the hippocampus is first affected. Age (more than 65), hereditary, and genetic information (ε4 allele of Apolipoprotein E) are directly linked to Alzheimer's [2]. Diabetes mellitus, cardiovascular diseases, brain injury, and brain trauma are the most common reasons for Alzheimer's disease. Recently, researchers in China reported the first young patient of Alzheimer's disease at the age of 19. The gradual amassing of the beta-amyloid protein fragment (senile plaques) and hyperphosphorylated, aggregated tau proteins (neurofibrillary tangles) are the key features of AD pathogenesis [3]. Scientists identified the role of gamma-secretase, acetylcholinesterase, butyrylcholinesterase, and glycogen synthase kinase-3beta enzymes in the treatment of Alzheimer's disease. Gamma secretase is a combination of presenilin, nicastrin, Aph-1, and Pen-2 proteins. Inhibition of the Notch signaling pathway by gamma-secretase inhibitors shows side effects. Gamma secretase inhibitors cleaved amyloid precursor protein associated with Alzheimer's disease [4]. The increased levels of acetylcholine by the inhibitions of acetylcholinesterase and butyrylcholinesterase enzymes, the occurrence and viability of Alzheimer's disease were treated [5]. Glycogen synthase kinase-3 enzyme is a serine-threonine-based enzyme with two subtypes: GSK-3α and GSK-3β. The enzyme is mainly associated with activation of downregulation of neurons using phosphorylation of serine21 (GSK-3α) and serine9 (GSK-3β). GSK-3α linked with the generation of beta-amyloid plaque, hyperphosphorylation of tau protein, and activation of microglial cells, which finally generate neurotoxic inflammation with a reduced amount of acetylcholine; these factors collectively cause Alzheimer's disease [6]. Alzheimer's and progressive supranuclear palsy caused by the accretion of tau protein. These diseases are also caused by the binding of tau protein to microtubules. The stabilization of the microtubule depends upon acetylation, and Histone Deacetylase-6 (HDAC6) positively regulates the acetylation of the microtubule, so inhibition of the enzyme improves axonal activity and attenuates the progression of Alzheimer's [7]. A recent study stated that one drug can interact with three targets as well, and one target has about 4.7 drugs, indicating that polypharmacology is a common phenomenon and basis for repurposing drugs. Thus, computer-aided drug design (CADD) and polypharmacology allow rational identification of an FDA-approved drug for pursuing targets other than previously established ones [8]. In this manuscript, we selected a series of nonselective HDAC inhibitors and targeted against gamma-secretase, Acetylcholinesterase, Butyrylcholinesterase, and Glycogen Synthase Kinase-3β enzymes to identify the best molecule and rerouting HDAC inhibitors in the treatment of Alzheimer disease.

2. Materials and Methods

2.1. Data collection and filtration.

A total of 60 HDAC inhibitors (HDACI) and Rivastigmine (Table 1) were collected from literature and transferred to the SWISS ADME portal to identify the molecules that were able to cross the Blood Brain Barrier (BBB), pass through Lipinski and Ghose filters as most of the molecules were targeted to brain to treat Alzheimer disease, so these filters were the essential part of the research to reduce the dataset for further drug-receptor interactions (Figure 1) (Table 2) [9].

Table 1. Smile notification of the selected HDAC inhibitors and Rivastigmine.

S.No	Molecule	IUPAC	Smile
1	Rivastigmine (standard)	[3-[(1S)-1-(dimethylamino)ethyl]phenyl] N-ethyl-N-methylcarbamate	CCN(C)C(=O)OC1=CC=CC(=C1)[C@H](C)N(C)C
2	Trichostatin A	(2E,4E,6R)-7-[4-(dimethylamino)phenyl]-N-hydroxy-4,6-dimethyl-7-oxohepta-2,4-dienamide	C[C@H](/C=C(\C)/C=C/C(=O)NO)C(=O)C1=CC=C(C=C1)N(C)C
3	Psammaplin A	(2E)-3-(3-bromo-4-hydroxyphenyl)-N-[2-[2-[[(2E)-3-(3-bromo-4-hydroxyphenyl)-2-hydroxyiminopropanoyl]amino]ethyldisulfanyl]ethyl]-2-hydroxyiminopropanamide	C1=CC(=C(C=C1C/C(=N\O)/C(=O)NCCSSCCNC(=O)/C(=N/O)/CC2=CC(=C(C=C2)O)Br)Br)O
4	Romidepsin	(1S,4S,7Z,10S,16E,21R)-7-ethylidene-4,21-di(propan-2-yl)-2-oxa-12,13-dithia-5,8,20,23-tetrazabicyclo[8.7.6]tricos-16-ene-3,6,9,19,22-pentone	C/C=C\1/C(=O)N[C@H](C(=O)O[C@H]\2CC(=O)N[C@@H](C(=O)N[C@H](CSSCC/C=C2)C(=O)N1)C(C)C)C(C)C
5	Spiruchostatin A	1S,5S,6R,9S,15E,20R)-5-hydroxy-20-methyl-6-propan-2-yl-2-oxa-11,12-dithia-7,19,22-triazabicyclo[7.7.6]docos-15-ene-3,8,18,21-tetron	C[C@@H]1C(=O)N[C@@H]2CSSCC/C=C/[C@H](CC(=O)N1)OC(=O)C[C@@H]([C@H](NC2=O)C(C)C)O
6	Largazole	S-[(E)-4-[(5R,8S,11S)-5-methyl-6,9,13-trioxo-8-propan-2-yl-10-oxa-3,17-dithia-7,14,19,20-tetrazatricyclo[14.2.1.12,5]icosa-1(18),2(20),16(19)-trien-11-yl]but-3-enyl] octanethioate	CCCCCCCC(=O)SCC/C=C/[C@@H]1CC(=O)NCC2=NC(=CS2)C3=N[C@@](CS3)(C(=O)N[C@H](C(=O)O1)C(C)C)C
7	Azumamide E	(Z)-6-[(2R,5R,8R,11R,12S)-8-benzyl-5,12-dimethyl-3,6,9,13-tetraoxo-2-propan-2-yl-1,4,7,10-tetrazacyclotridec-11-yl]hex-4-enoic acid	C[C@H]1[C@H](NC(=O)[C@H](NC(=O)[C@H](NC(=O)[C@H](NC1=O)C(C)C)C)CC2=CC=CC=C2)C/C=C\CCC(=O)O
8	Trapoxin A	(3S,6S,9S,12R)-3,6-dibenzyl-9-[6-[(2S)-oxiran-2-yl]-6-oxohexyl]-1,4,7,10-tetrazabicyclo[10.4.0]hexadecane-2,5,8,11-tetrone	C1CCN2[C@H](C1)C(=O)N[C@H](C(=O)N[C@H](C(=O)N[C@H](C2=O)CC3=CC=CC=C3)CC4=CC=CC=C4)CCCCCC(=O)[C@@H]5CO5
9	vorinostat	N'-hydroxy-N-phenyloctanediamide	C1=CC=C(C=C1)NC(=O)CCCCCCC(=O)NO
10	Tefinostat	cyclopentyl (2S)-2-[[4-[[8-(hydroxyamino)-8-oxooctanoyl]amino]phenyl]methylamino]-2-phenylacetate	C1CCC(C1)OC(=O)[C@H](C2=CC=CC=C2)NCC3=CC=C(C=C3)NC(=O)CCCCCCC(=O)NO
11	CG200745	(E)-N-[3-(dimethylamino)propyl]-N'-hydroxy-2-(naphthalen-1-yloxymethyl)oct-2-enediamide	CN(C)CCCNC(=O)/C(=C/CCCCC(=O)NO)/COC1=CC=CC2=CC=CC=C21

S.No	Molecule	IUPAC	Smile
12	Ricolinostat	N-[7-(hydroxyamino)-7-oxoheptyl]-2-(N-phenylanilino)pyrimidine-5-carboxamide	C1=CC=C(C=C1)N(C2=CC=CC=C2)C3=NC=C(C=N3)C(=O)NCCCCCCC(=O)NO
13	Citarinostat	2-(N-(2-chlorophenyl)anilino)-N-[7-(hydroxyamino)-7-oxoheptyl]pyrimidine-5-carboxamide	C1=CC=C(C=C1)N(C2=CC=CC=C2Cl)C3=NC=C(C=N3)C(=O)NCCCCCCC(=O)NO
14	CUDC-101	7-[4-(3-ethynylanilino)-7-methoxyquinazolin-6-yl]oxy-N-hydroxyheptanamide	COC1=C(C=C2C(=C1)N=CN=C2NC3=CC=CC(=C3)C#C)OCCCCCCC(=O)NO
15	Tinostamustine	7-[5-[bis(2-chloroethyl)amino]-1-methylbenzimidazol-2-yl]-N-hydroxyheptanamide	CN1C2=C(C=C(C=C2)N(CCCl)CCCl)N=C1CCCCCCC(=O)NO
16	Belinostat	(E)-N-hydroxy-3-[3-(phenylsulfamoyl)phenyl]prop-2-enamide	C1=CC=C(C=C1)NS(=O)(=O)C2=CC=CC(=C2)/C=C/C(=O)NO
17	Panobinostat	(E)-N-hydroxy-3-[4-[[2-(2-methyl-1H-indol-3-yl)ethylamino]methyl]phenyl]prop-2-enamide	CC1=C(C2=CC=CC=C2N1)CCNCC3=CC=C(C=C3)/C=C/C(=O)NO
18	Resminostat	(E)-3-[1-[4-[(dimethylamino)methyl]phenyl]sulfonylpyrrol-3-yl]-N-hydroxyprop-2-enamide	CN(C)CC1=CC=C(C=C1)S(=O)(=O)N2C=CC(=C2)/C=C/C(=O)NO
19	Pracinostat	(E)-3-[2-butyl-1-[2-(diethylamino)ethyl]benzimidazol-5-yl]-N-hydroxyprop-2-enamide	CCCCC1=NC2=C(N1CCN(CC)CC)C=CC(=C2)/C=C/C(=O)NO
20	Givinostat	[6-(diethylaminomethyl)naphthalen-2-yl]methyl N-[4-(hydroxycarbamoyl)phenyl]carbamate	CCN(CC)CC1=CC2=C(C=C1)C=C(C=C2)COC(=O)NC3=CC=C(C=C3)C(=O)NO
21	Abexinostat	3-[(dimethylamino)methyl]-N-[2-[4-(hydroxycarbamoyl)phenoxy]ethyl]-1-benzofuran-2-carboxamide	CN(C)CC1=C(OC2=CC=CC=C21)C(=O)NCCOC3=CC=C(C=C3)C(=O)NO
22	AR-42	N-hydroxy-4-[[(2S)-3-methyl-2-phenylbutanoyl]amino]benzamide	CC(C)[C@@H](C1=CC=CC=C1)C(=O)NC2=CC=C(C=C2)C(=O)NO
23	Bisthianostat	5-cyclopropyl-N-[5-(hydroxyamino)-5-oxopentyl]-2-(1,3-thiazol-2-yl)-1,3-thiazole-4-carboxamide	C1CC1C2=C(N=C(S2)C3=NC=CS3)C(=O)NCCCCC(=O)NO
24	Quisinostat	N-hydroxy-2-[4-[[(1-methylindol-3-yl)methylamino]methyl]piperidin-1-yl]pyrimidine-5-carboxamide	CN1C=C(C2=CC=CC=C21)CNCC3CCN(CC3)C4=NC=C(C=N4)C(=O)NO
25	Nanatinostat	2-[(1S,5R)-6-[(6-fluoroquinolin-2-yl)methylamino]-3-azabicyclo[3.1.0]hexan-3-yl]-N-hydroxypyrimidine-5-carboxamide	C1[C@@H]2[C@@H](C2NCC3=NC4=C(C=C3)C=C(C=C4)F)CN1C5=NC=C(C=N5)C(=O)NO
26	Fimepinostat	N-hydroxy-2-[[2-(6-methoxypyridin-3-yl)-4-morpholin-4-ylthieno[3,2-d]pyrimidin-6-yl]methyl-methylamino]pyrimidine-5-carboxamide	CN(CC1=CC2=C(S1)C(=NC(=N2)C3=CN=C(C=C3)OC)N4CCOCC4)C5=NC=C(C=N5)C(=O)NO
27	Tacedinaline	4-acetamido-N-(2-aminophenyl)benzamide	CC(=O)NC1=CC=C(C=C1)C(=O)NC2=CC=CC=C2N
28	Entinostat	pyridin-3-ylmethyl N-[[4-[(2-aminophenyl)carbamoyl]phenyl]methyl]carbamate	C1=CC=C(C(=C1)N)NC(=O)C2=CC=C(C=C2)CNC(=O)OCC3=CN=CC=C3
29	Mocetinostat	N-(2-aminophenyl)-4-[[(4-pyridin-3-ylpyrimidin-2-yl)amino]methyl]benzamide	C1=CC=C(C(=C1)N)NC(=O)C2=CC=C(C=C2)CNC3=NC=CC(=N3)C4=CN=CC=C4
30	Tucidinostat	N-(2-amino-4-fluorophenyl)-4-[[[(E)-3-pyridin-3-ylprop-2-enoyl]amino]methyl]benzamide	C1=CC(=CN=C1)/C=C/C(=O)NCC2=CC=C(C=C2)C(=O)NC3=C(C=C(C=C3)F)N
31	Domatinostat	(E)-N-(2-aminophenyl)-3-[1-[4-(1-methylpyrazol-4-yl)phenyl]sulfonylpyrrol-3-yl]prop-2-enamide	CN1C=C(C=N1)C2=CC=C(C=C2)S(=O)(=O)N3C=CC(=C3)/C=C/C(=O)NC4=CC=CC=C4N
32	CXD101	N-(2-aminophenyl)-4-[1-[(1,3-dimethylpyrazol-4-yl)methyl]piperidin-4-yl]benzamide	CC1=NN(C=C1CN2CCC(CC2)C3=CC=C(C=C3)C(=O)NC4=CC=CC=C4N)C
33	Analog 33	(3R,9S,12R,16R,E)-6- ethylidene-3,12-diisopropyl-9-methyl-16-propyl-	C[C@H](N1)C(N/C(C(N[C@@H](C(C)C)C(O[C@@H](CC(N[C@H](C(C)C)C1=O)=O)CCC)=O)=O)=C/C)=O analog33

S.No	Molecule	IUPAC	Smile
		1-oxa-4,7,10,13-tetraazacyclohexadecane-2,5,8,11,14-pentaone	
34	Analog34	(S)-2-amino-3-(3,5-dichlorophenyl)-1-(isoindolin-2-yl)propan-1-one	O=C(N1CC2=C(C=CC=C2)C1)[C@@H](N)CC3=CC(Cl)=CC(Cl)=C3 analog34
35	Analog35	N-hydroxycyclopent-1-enecarboxamide	ONC(C1=CCCC1)=O analog35
36	Analog36	4-bromo-N'-butylbenzohydrazide	O=C(NNCCCC)C1=CC=C(Br)C=C1 analog36
37	Analog37	2,2,3,3,4,4,5,5,6,6-decafluoro-N^8-hydroxy-7,7-dimethyl-N^1-phenyloctanediamide	ONC(C(C)(C)C(F)(F)C(F)(F)C(F)(F)C(F)(F)C(F)(F)C(NC1=CC=CC=C1)=O)=O analog37
38	Analog38	9,10-dihydrobenzo[e]pyrimidol[1,2-c][1,3]thiazin-1(8H)-imine	N=C1SC2=CC=CC=C2C3=NCCCN13 analog38
39	Analog39	4-hydroxy-5-methoxy-N,1-dimethyl-2-methylene-N-(4-(trifluoromethyl)phenyl)-1,2-dihydroquinoline—carboxamide	O=C(C1=C(O)C2=C(N(C)C1=C)C=CC=C2OC)N(C)C3=CC=C(C(F)(F)F)C=C3 analog39
40	Analog40	4-acetamido-N(2-amino-5-(thiophen-2-yl)phenyl) benzamide	CC(NC1=CC=C(C(NC2=C(N)C=CC(C3=CC=CS3)=C2)=O)C=C1)=O analog40
41	Analog41	N-(2-amino-5-(thiophen-2-yl)phenyl)-6-(2-oxo-1-oxa-,8-diazaspiro[4,5]decan-8-yl)nicotinamide	O=C(NC1=C(N)C=CC(C2=CC=CS2)=C1)C(C=C3)=CN=C3N(CC4)CC[C@@]4(O5)CNC5=O analog41
42	Analog42	N-(2-amino-5-(thiophen-2-yl)phenyl)-2-(piperazin-1-yl)quinolone-6-carboxamide	NC1=C(C=C(C2=CC=CS2)C=C1)NC(C3=CC=C4C(C=CC(N5CCNCC5)=N4)=C3)=O analog42
43	Analog43	N-(4-((4-amino-4'-fluoro-[1,1'-biphenyl]-3-yl)carbomoyl)phenyl)tertrahydro-2H-pyran-4-carboxamide	O=C(NC1=CC=C(C(NC2=C(N)C=CC(C3=CC=C(F)C=C3)=C2)=O)C=C1)C4CCOCC4 analog43
44	Analog44	4-acetamido-N-(2-amino-4-fluorophenyl)benzamide	CC(NC1=CC=C(C(NC2=C(N)C=C(F)C=C2)=O)C=C1)=O analog44
45	Analog45	(E)-N-(2-amino-4-fluorophenyl)-3-(1-cinnamyl-1H-1,2,3-triazol-4-yl)acrylamide	O=C(NC1=CC=C(F)C=C1N)/C=C/C2=CN(C/C=C/C3=CC=CC=C3)N=N2 analog45
46	Analog46	(S)-7-(2-(5-cyano-1H-indol-1-yl)acetamido)-7(5-(4-((dimethylamino)methyl)phenyl)-1H-imidazol-2-yl)-N-methylheptanamide	CN(C)CC1=CC=C(C=C1)C2=CN=C(N2)[C@H](CCCCCC(NC)=O)NC(CN(C=C3)C4=C3C=C(C#N)C=C4)=O analog46
47	Analog47	N-hydroxy-4-((2-methyl-3,4-dihydro-1H-pyrido[4,3-b]indol-5(2H)-yl)methyl)benzamide	ONC(C(C=C1)=CC=C1CN(C2=C3C=CC=C2)C4=C3CN(C)CC4)=O analog47
48	Analog48	4-((6-chloro-3,4-dihydroquinolin-1(2H)-yl)methyl)-N-hydroxybenzamie	O=C(NO)C1=CC=C(CN2CCCC3=C2C=CC(Cl)=C3)C=C1 analog48
49	Analog49	N-hydroxy-4-((quinolone-8-ylamino)methyl)benzamide	ONC(C(C=C1)=CC=C1CNC2=CC=CC3=C2N=CC=C3)=O analog49
50	Analog50	2-(4,4-difluoro-1-phenylcyclohexyl)-N-hydroxypyrimidine-5-carboxamide	FC(CC1)(F)CCC1(C2=NC=C(C(NO)=O)C=N2)C3=CC=CC=C3 analog50
51	Analog51	(E)-N-hydroxy-3-(5-methoxy-[1,1':4',1''-terphenyl]-2-yl)acrylamide	COC1=CC(C2=CC=C(C=C2)C3=CC=CC=C3)=C(/C=C/C(NO)=O)C=C1 analog51
52	Analog52	(S)-4-((N-butyl-2-(4((5-(4-(((2-(2,6-dioxopiperidine-3-yl)-1,3-dioxoisoindolin-7-yl)amino)methyl)-1H-1,2,3-triazol-1yl)pentyl)oxy)phenyl)acetamido)methyl)-N-hydroxybenzamide	O=C(N1)[C@@H](N2C(C3=C(NCC4=CN(CCCCCOC5=CC=C(CC(N(CCCC)CC6=CC=C(C(NO)=O)C=C6)=O)C=C5)N=N4)C=CC=C3C2=O)=O)CCC1=O analog52
53	Analog53	(E)-2-(5-(2-cyclopropylvinyl)-4-phenyl-1H-1,2,3-triazol-1-yl)-N-hydroxy-3-phenylpropanamide compound with ethane (1:1)	ONC(C(N1C(/C=C/C2CC2)=C(C3=CC=CC=C3)N=N1)CC4=CC=CC=C4)=O.CC analog53
54	Analog54	N-hydroxy-1,1-dimethyl-2-(5-(trifluoromethyl)pyrazin-2-yl)isoindoline-4-carboxamide	ONC(C1=C2C(C(C)(C)N(C2)C3=CN=C(C(F)(F)F)C=N3)=CC=C1)=O analog54
55	Analog55	N'-hexadecylthiophene-2-carbohydrazide	O=C(NNCCCCCCCCCCCCCCCC)C1=CC=CS1 analog55
56	Analog56	4-((3-((hydroxyl(methyl)amino)-1H-indol-1-yl)methyl)-N-methylbenzamide	CN(C)CC1=CN(CC2=CC(C(NO)=O)=CC=C2)C3=CC=CC=C31 analog56

S.No	Molecule	IUPAC	Smile
57	Analog57	N-methyl-4-((3-(pyrrolidin-1-ylmethyl)-1H-indol-1-yl)methyl)benzamide	CNC(C1=CC=C(CN2C(C=CC=C3)=C3C(CN4CCCC4)=C2)C=C1)=O analog57
58	Analog58	6-((3-aminopropyl)amino)-N-hydroxyhexanamide	NCCCNCCCCCC(NO)=O analog58
59	Analog59	N-((4-(4-phenythiazol-2-yl)tetrahydro-2H-pyran-4-yl)methyl)-3-(5-(trifluoromethyl)-1,2,3-oxadiazole-3-yl)benzamide	O=C(C1=CC=CC(C2=NOC(C(F)(F)F)=N2)=C1)NCC3(CCOCC3)C4=NC(C5=CC=CC=C5)=CS4 analog59
60	Analog60	(1S,2R,3S)-1-fluoro-2-(4-(5-fluoropyrimidin-2-yl)phenyl)-N-hydroxy-3-phenyl)-N-hydroxy-3-phenylcyclopropanecarboxamide	F[C@]1(C(NO)=O)[C@H]([C@H]1C2=CC=CC=C2)C3=CC=C(C=C3)C4=NC=C(F)C=N4 analog60
61	Analog61	(R)-2-(2-fluorophenyl)-N-hyroxy-2-(4-(4-(5-(trifluoromethyl)pyrimidin-2-yl)phenylsulfonamido)phenyl)acetamide	ONC([C@@H](C1=CC=CC=C1F)C2=CC=C(C=C2)NS(C3=CC=C(C=C3)C4=NC=C(C(F)(F)F)C=N4)(=O)=O)=O analog61

Table 2. SWISS-ADME data of the HDAC inhibitors and Rivastigmine.

S. N	Molecule	MW	NRB	HBA	HBD	MR	TPSA	iLP	XLP	WLP	MLP	BBBP	LKP	LV
1	Rivastigmine (standard)	250.34	6	3	0	73.12	32.78	3.2	2.29	2.44	2.34	Yes	-6.2	0
2	Trichostatin A	302.37	7	3	2	87.28	69.64	1.9	2.75	2.58	2.01	Yes	-6.19	0
3	Psammaplin A (b)	664.39	15	8	6	148.62	214.44	2.6	4.78	3.68	1.63	No	-6.96	2
4	Romidepsin	540.7	2	6	4	156.44	193.3	3.24	2.24	-0.09	0.18	No	-8.01	1
5	Spiruchostatin A	473.61	1	6	4	131.93	184.43	1.92	0.39	-0.62	-0.16	No	-8.91	0
6	Largazole	622.86	12	7	2	180.26	205.66	4.99	5.47	3.74	1.3	No	-6.22	1
7	Azumamide E	514.61	8	6	5	154.4	153.7	2.6	2.41	-0.22	0.64	No	-7.73	1
8	Trapoxin A	602.72	11	6	3	179.55	137.21	2.9	3.42	0.72	1.02	No	-7.55	1
9	vorinostat	264.32	10	3	3	73.33	78.43	1.84	1.86	2.28	1.83	No	-6.59	0
10	Tefinostat	495.61	17	6	4	138.4	116.76	4.15	3.84	4.12	2.66	No	-6.6	0
11	CG200745	427.54	15	5	3	122.09	90.9	3.34	3.04	3.28	2.25	No	-6.75	0
12	Ricolinostat	433.5	13	6	3	122.28	107.45	2.7	3.42	4.13	2.5	No	-6.52	0
13	Citarinostat	467.95	13	5	3	127.29	107.45	3.62	4.05	4.79	2.71	No	-6.28	0
14	CUDC-101	434.49	12	5	3	122.57	105.6	3.82	3.98	4.28	2.67	No	-6.12	0
15	Tinostamustine	415.36	13	5	2	111.95	70.39	3.43	3.6	3.86	2.74	Yes	-6.28	0
16	Belinostat	318.35	6	6	3	82.18	103.88	0.61	1.66	2.79	1.55	No	-7.06	0
17	Panobinostat	349.43	8	3	4	103.76	77.15	2.38	2.99	3.07	2.31	Yes	-6.31	0
18	Resminostat	349.4	7	5	2	89.61	100.02	2.46	0.94	2.13	1.46	No	-7.76	0
19	Pracinostat	358.48	11	4	2	105.94	70.39	3.35	3.09	3.13	2.17	Yes	-6.29	0
20	Givinostat	421.49	11	5	3	120.23	90.9	3.62	3.6	4.05	3.18	No	-6.32	0
21	Abexinostat	397.42	10	6	3	106.42	104.04	3.18	2.23	2.27	1.12	No	-7.14	0
22	AR-42	312.36	7	3	3	88.58	78.43	2.35	2.85	2.99	2.84	Yes	-6.18	0
23	Bisthianostat	366.46	10	5	3	91.64	160.69	2.52	1.34	2.49	0.18	No	-7.58	0
24	Quisinostat	394.47	7	5	3	114.06	95.31	2.4	1.33	1.56	1.33	No	-7.76	0
25	Nanatinostat	394.4	6	7	3	105.64	103.27	2.87	1.04	1.39	1.45	No	-15.73	0
26	Fimepinostat	508.55	8	9	2	136.07	166.96	2.94	1.34	1.61	0.1	No	-8.45	2
27	Tacedinaline	269.3	5	2	3	79.37	84.22	1.7	1.25	2.11	1.84	No	-7.06	0
28	Entinostat	376.41	9	4	3	106.4	106.34	2.04	2.02	2.86	1.57	No	-7.16	0
29	Mocetinostat	396.44	7	4	3	117.67	105.82	2.59	2.76	3.46	1.72	No	-6.76	0
30	Tucidinostat	390.41	8	4	3	110.01	97.11	2.51	2.3	3.36	2.08	No	-7.05	0
31	Domatinostat	447.51	7	4	2	124.31	120.39	2.6	2.41	4.15	2.42	No	-7.32	0
32	CXD101	403.52	6	3	2	125.26	76.18	3.2	2.86	3.23	2.71	Yes	-6.73	0
33	Analog 33	466.57	4	6	4	139.04	142.7	3.39	2.52	-0.61	0.05	No	-7.36	0
34	Analog34	333.21	4	2	1	90.45	48.02	2.91	4.13	4.16	3.47	Yes	-5.4	0
35	Analog35	129.16	2	2	2	32.57	49.33	1.44	0.59	0.68	0.41	Yes	-6.67	0
36	Analog36	271.15	6	2	2	64.36	41.13	2.41	2.91	2.48	3.06	Yes	-5.89	0
37	Analog37	504.53	4	14	8	112.23	84.58	0	8.15	11.81	3.91	No	-3.59	1
38	Analog38	221.32	2	2	1	74.96	66.92	1.88	1.12	0.53	1.89	No	-6.85	0
39	Analog39	418.49	9	7	3	109.81	66.65	4.53	3.45	4.35	1.81	Yes	-6.4	0
40	Analog40	353.44	4	2	3	103.01	126.45	2.93	2.56	3.56	1.95	No	-6.64	0
41	Analog41	462.63	7	7	2	142.58	124.61	0	3.17	3.45	2.25	No	-6.87	0
42	Analog42	437.6	10	3	4	134.29	120.31	0	4.08	4.53	2.23	No	-6.07	0
43	Analog43	445.57	8	4	3	130.67	93.45	6.88	3.24	4.68	2.39	No	-6.72	0

S. N	Molecule	MW	NRB	HBA	HBD	MR	TPSA	iLP	XLP	WLP	MLP	BBBP	LKP	LV
44	Analog44	287.29	5	3	3	79.33	84.22	1.77	1.35	2.67	2.23	No	-7.09	
45	Analog45	381.53	6	5	3	123.88	64.61	0	4.15	3.36	2.64	Yes	-5.68	
46	Analog46	549.75	10	8	8	162.9	166.92	0	0.84	3.61	0.6	No	-9.06	2
47	Analog47	347.49	1	2	1	115.38	64.25	0	4.99	2.53	1.19	Yes	-4.88	0
48	Analog48	326.86	5	2	3	92.67	61.36	4.31	3.5	4.1	2.84	Yes	-5.81	0
49	Analog49	293.32	5	3	3	84.45	74.25	1.71	2.46	2.62	1.96	Yes	-6.34	0
50	Analog50	345.43	9	7	5	93.67	76.55	3.27	1.6	2.09	1.52	No	-7.27	0
51	Analog51	345.39	6	3	2	102.44	58.56	2.78	4.36	4.44	3.68	Yes	-5.31	0
52	Analog52	787.92	17	12	5	220.98	220	0	5.1	3.92	2.82	No	-7.49	2
53	Analog53	374	10	4	3	113.58	75.24	3.8	5.07	4.23	2.73	No	-5.08	0
54	Analog54	352.31	4	7	2	84.51	80.04	3.49	2.77	4.67	1.71	No	-6.48	0
55	Analog55	368.62	15	2	2	114.34	69.37	6.1	8.94	6.71	4.51	No	-2.2	1
56	Analog56	331.45	7	4	3	100.17	78.36	0	1.2	2.31	2.25	No	-7.47	0
57	Analog57	347.41	5	4	3	105.77	76.19	0	1.25	2.39	2.38	Yes	-7.53	0
58	Analog58	215.38	1	4	4	67.3	87.38	0	0.09	1.47	0.12	No	-7.55	0
59	Analog59	550.81	7	9	7	155.86	131.07	0	5.63	6.54	1.84	No	-5.66	1
60	Analog60	393.56	1	6	3	125.6	74.28	0	5.42	4.87	3.24	No	-4.85	0
61	Analog61	574.72	4	10	5	154.57	151.09	0	5.42	7.97	3.24	No	-4.85	0

MW: Molecular Weight, NRB: Number of Rotatable bonds, HBA: Hydrogen bond acceptors, HBD: Hydrogen bond donors, LV: Lipinski Rule Violation, LKP: log Kp (cm/s), BBBP: BBB permeability, MLP: MLOGP, WLP: WLOGP, XLP: XLOGP, iLP: iLOGP, MR: Molar Refractivity, TPSA: Topological Polar Surface Area.

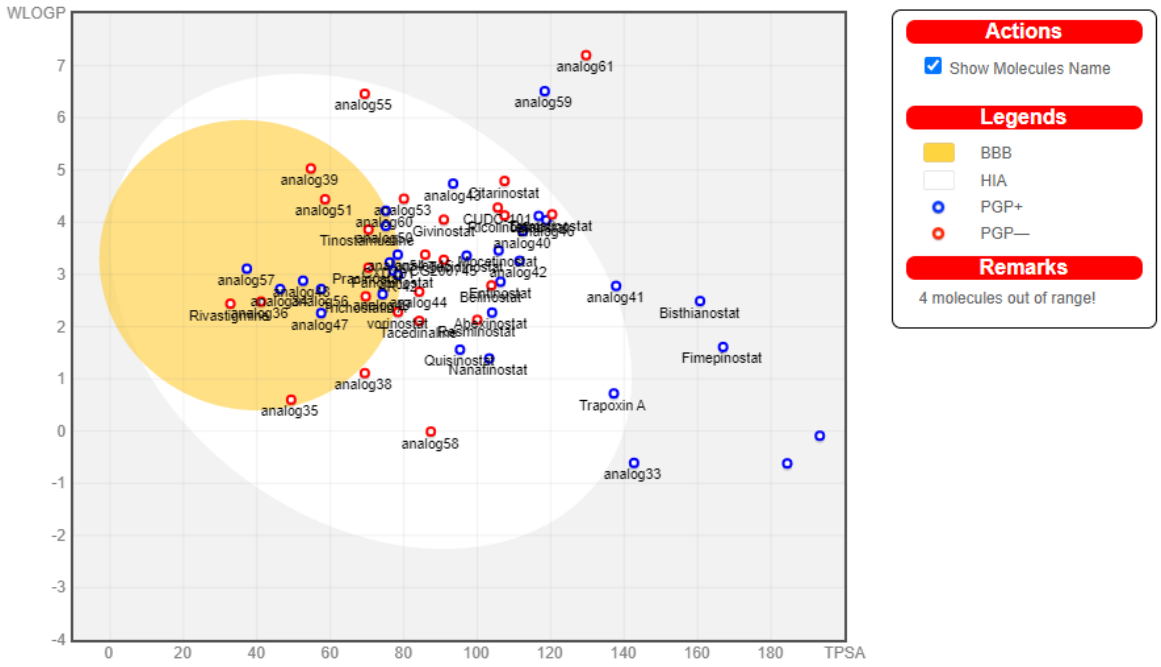

Figure 1 Swiss ADME boiled egg diagram highlighting molecules cross BBB and other parameters.

2.2. Molecular docking study.

2.2.1. Selection and preparation of the receptor.

A molecular docking study was used to predict the ligand-target interactions by calculating binding energy. In the molecular docking study, ligand and target protein interacted to create an environment to inhibit the ligand molecules' receptor activity, and the output features reflected the possible activity of the ligand molecule. The interactive pose of the ligand molecules within the receptor reflected the structural features of the ligand upon interaction with the receptor. The output energy tabulation represented the highest to lowest docking conformers [10]. In this study, HDACI(s) were docked against 6LQG, 7AIT, 6QAE, and 3GB2

receptors to evaluate the inhibitory activities against gamma-secretase, acetylcholinesterase, butyrylcholinesterase, and glycogen synthase kinase-3 beta enzymes to assess anti-Alzheimer activity. 6LQG receptor belongs to human gamma-secretase in co-crystallized with small molecule Avagacestat [11]. 7AIT receptor belongs to the crystal structure of Torpedo californica acetylcholinesterase co-crystallized with 7-[(3-Chloro-6,7,10,11-tetrahydro-9-methyl-7,11-methanocycloocta[b]quinolin-12-yl)amino]-N-(4-hydroxy-3-methoxybenzyl)heptanamide as inhibitor [12]. 6QAE receptor belongs to human butyrylcholinesterase bound with (S)-N2-butyl-N1-(2-cycloheptylethyl)-3-(1H-indol-3-yl)-N1,N2-dimethylpropane-1,2-diamine [13]. 3GB2 receptor is the glycogen synthase kinase-3beta receptor complexed with 2-methyl-5-(3-{4-[(S)-methylsulfinyl]phenyl}-1-benzofuran-5-yl)-1,3,4-oxadiazole as ligand [14]. Before proceeding with molecular docking studies, receptors were checked for missing residues using PyMol software, followed by maintaining the ionization state of the amino acids in the receptor using the H^{++} server. Then, the surrounding residues of the co-crystallized ligands were evaluated by Drug Discovery Studio. The molecular docking study was performed by AUTODOCK Vina software and visualized by Drug Discovery Studio software.

2.2.2. Preparation of ligand molecules.

The structures of the HDACI(s) [Rivastigmine, Trichostatin A, Tinostamustine, Panobinostat, Pracinostat, Abexinostat, (S)-2-amino-3-(3,5-dichlorophenyl)-1-(isoindolin-2-yl)propan-1-one, N-hydroxycyclopent-1-enecarboxamide, 4-bromo-N'-butylbenzohydrazide, 4-hydroxy-5-methoxy-N,1-dimethyl-2-methylene-N-(4-(trifluoromethyl)phenyl)-1,2-dihydroquinoline-3-carboxamide, (E)-N-(2-amino-4-fluorophenyl)-3-(1-cinnamyl-1H-1,2,3-triazol-4-yl)acrylamide, N-hydroxy-4-((2-methyl-3,4-dihydro-1H-pyrido[4,3-b]indol-5(2H)-yl)methyl)benzamide, 4-((6-chloro-3,4-dihydroquinolin-1(2H)-yl)methyl)-N-hydroxybenzamide, N-hydroxy-4-((quinolin-8-ylamino)methyl)benzamide, (E)-N-hydroxy-3-(5-methoxy-[1,1':4',1''-terphenyl]-2-yl)acrylamide, and N-methyl-4-((3-(pyrrolidin-1-ylmethyl)-1H-indol-1-yl)methyl)benzamide] were developed using Avogadro software. The molecule was optimized using MMFF94 and the steepest descent methods. Then, all the three-dimensional coordinates were added to the structure using Open Babel software. The total energy of the ligand was minimized using a Swiss pdb viewer with the 20 steepest decent processes [15]. Then, all the polar hydrogens and gasteiger charges were added to the molecules using AUTODOCK Vina and saved in PDBQT format.

2.2.3. Molecular docking parameter of the molecules interacted with the receptors.

Receptor and ligand molecules were charged with gasteiger charge and saved in pdbqt format. The Lamarckian genetic algorithm was applied to seek the best binding site of ligands in respective proteins. Protein-ligand docking default parameters with the grid box dimensions are listed below. Conformations were set as output for the ligand-protein docking experiments. Finally, the docking results were visualized and analyzed using BIOVIA Discovery Studio Visualizer 4.5 and Ligplus [16]. The grid box size of the 6LQG receptor was center_x = 166.923, center_y = 175.995, center_z = 153.272; size_x = 24, size_y = 24, size_z = 24 with exhaustiveness = 8. The grid box size of the 7AIT receptor was center_x = -0.142, center_y = 49.924, center_z = 53.679; size_x = 24, size_y = 24, size_z = 24 with exhaustiveness = 8. The grid box size of the 6QAE receptor was center_x = 137.7, center_y = 111.794, center_z =

38.383; size_x = 24, size_y = 24, size_z = 24 with exhaustiveness = 8. The grid box size of the 3GB2 receptor was center_x = 40.144, center_y = 17.98, center_z = -0.341; size_x = 24, size_y = 24, size_z = 24 with exhaustiveness = 8.

2.3. Osiris-molinspiration profiling.

In-silico prediction of cLogP, solubility, molecular weight, topological polar surface area, drug-likeness, drug score, mutagenic risk, tumorigenic risk, irritant risk, reproduction risk, and in-silico bioactivity of HDAC inhibitors was assessed by OSIRIS and MOLINSPIRATION software, respectively [17].

2.4. Frontier molecular orbital (FMO) analysis.

The frontier molecular orbital (FMO) analysis of the Analog 57 [N-methyl-4-((3-(pyrrolidin-1-ylmethyl)-1H-indol-1-yl)methyl)benzamide] was performed using Becke-Lee-Parr hybrid exchange-correlation three-parameter functional (B3LYP) level with the standard 6-311G+(d,p) basis set on the basis of the optimized structure. Vibration analysis showed that the optimized structures were in accordance with the minimum points on the potential energy surface. All the convergent precisions were the system default values, and all calculations reported in this work were carried out using the Avogadro-ORCA software combination. In the same manner, Bond energy, angle energy, dihedral energy, electrostatic energy, and van der Waal energy of the molecule were calculated using AM1-BCC (quantum mechanics theory), 6-311++G** quantum mechanics basis with SAGE open force field initiative [18].

2.5. Molecular electrostatic potential (ESP) investigation.

The electrostatic potential is the representation of interaction energy within a specific zone of a structure. ESP is associated with the electrical charge distribution from the proton, nuclei, and electrons. The blue region represented the suitable site for nucleophilic attack, whereas the red region was associated with the site for electrophilic attack. The calculation is based on the B3LYP-6-31+ G(d,p) level process [19].

3. Results and Discussion

3.1. Data filtration.

The SWISS ADME data used LogP, LogS, Lipinski rule, Ghose Crippen filter, and BBB permeability as factors to filter the dataset. The results suggested that out of 60 HDAC inhibitors, 16HDAC inhibitors, and Rivastigmine passed through the filters, and further studies were carried out on the selected molecules.

3.2. Molecular docking study data.

As per the drug discovery studio data, 6LQG receptor co-crystallized with small molecule Avagacestat, which interacted with GLY 382 by hydrogen bond interaction; THR 421, ALA 431, LEU 432, PRO 433 by van der Waal interactions; LEU 425, LEU 418, LEU 422, ALA 434, LEU 381, VAL 272, LEU 268, LYS 380 by pi-pi interactions. The complexed ligand of 7AIT interacted with TYR 121 by hydrogen bond interaction; TYR 70, SER 81, GLY 118, GLY 119, GLU 199, SER 200, GLY 441, TY4 442 by van der Waal interactions; TRP 84, TRP 279, PHE 330, PHE 331, TYR 334, GLY 335 by pi-pi interactions. The complexed

ligand of 6QAEinteracted with TRP 82, TRP 231, PHE 329, GLY 116, TYR 332, TYR 332, and ALA 328 by pi-pi interactions. Complexed ligands of 3GB2 interacted with LYS 85 by hydrogen bond interaction; LEU 132, ASP 133, VAL 135, THR 138, ARG 141, by van der Waal interactions; VAL 70, ALA 83, CYS 199, PHE 67, ILE 62, LEU 188 by pi-pi interactions (Figure 2).

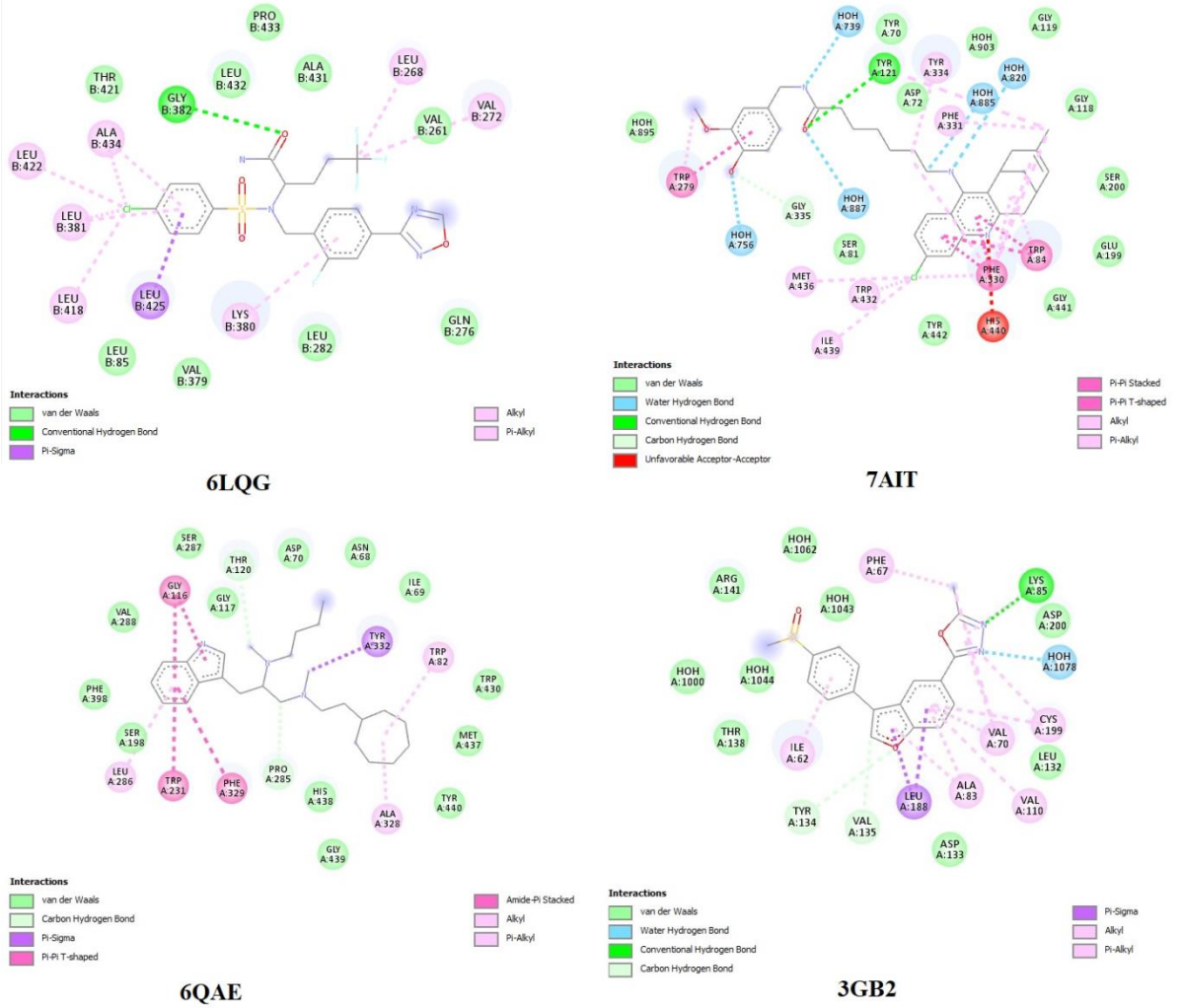

Figure 2. Surrounding and interacting residues for complexed ligands of 6LQG, 7AIT, 6QAE and 3GB2 receptors.

The molecular docking studies data generated after the interactions between selected HDACi(s) and 6LQG (gamma-secretase enzyme), 7AIT (acetylcholinesterase), 6QAE (butyrylcholinesterase), 3GB2 (glycogen synthase kinase-3beta) receptors; Analog 45 [(E)-N-(2-amino-4-fluorophenyl)-3-(1-cinnamyl-1H-1,2,3-triazol-4-yl)acrylamide] showed maximum docking interaction against 6LQG, 7AIT, 6QAE, 3GB2 with dock score of (-) 8.1 kcal/mol, (-) 10.5 kcal/mol, (-) 9.1 kcal/mol, (-) 7.3 kcal/mol, respectively. In the same experimental data, Analog 57 N-methyl-4-((3-(pyrrolidin-1-ylmethyl)-1H-indol-1-yl)methyl)benzamide also showed good molecular docking score of (-) 8.2 kcal/mol, (-) 11.5 kcal/mol, (-) 9.5 kcal/mol, and (-) 8.0 kcal/mol, respectively. Standard drug Rivastigmine showed docking score = (-) 5.3 kcal/mol [6LQG], (-) 8.0 kcal/mol [7AIT], (-) 7.2 kcal/mol [6QAE], (-) 6.1 kcal/mol [3GB2], respectively (Table 3) [19].

Table 3. Molecular docking interaction scores of the selected HDAC inhibitors and Rivastigmine against 6LQG, 7AIT, 6QAE, and 3GB2.

SN	Name of the Molecules	Dock Score (kcal/mol) 6LQG Gamma Secratase	Dock Score (kcal/mol) 7AIT AChE	Dock Score (kcal/mol) 6QAE BuChE	Dock Score (kcal/mol) 3GB2 GSK- 3β
1	Rivastigmine (standard)	-5.3	-8.0	-7.2	-6.1
2	Trichostatin A	-6.5	-8.9	-8.4	-7.3
3	Tinostamustine	-5.8	-8.6	-7.7	-7.0
4	Panobinostat	-6.8	-11.2	-9.7	-7.9
5	Pracinostat	-6.4	-9.4	-7.4	-6.7
6	Abexinostat	-7.4	-10.6	-10.0	-7.2
7	CXD101	-7.9	-9.8	-9.2	-7.5
8	Analog 34	-7.5	-10.7	-9.9	-7.6
9	Analog35	-4.6	-6.4	-5.9	-4.9
10	Analog36	-5.6	-7.8	-7.1	-6.3
11	Analog39	-8.0	-9.2	-9.6	-8.3
12	Analog45	-8.1	-10.5	-9.1	-7.3
13	Analog47	-7.9	-10.0	-9.3	-8.1
14	Analog48	-7.2	-9.4	-9.0	-8.1
15	Analog49	-6.9	-9.9	-9.8	-7.5
16	Analog51	-7.8	-10.9	-9.6	-8.2
17	Analog57	-8.2	-11.5	-9.5	-8.0

As per the interaction study data, (E)-N-(2-amino-4-fluorophenyl)-3-(1-cinnamyl-1H-1,2,3-triazol-4-yl)acrylamide interacted with 6LQG by Pi-sigma interaction with LEU282; by van der waal interactions with ASP257, LEU271, LEU150, PHE283, LEU286, ILE287, GLY382, LEU381, LYS380, THR421, LEU422, LEU425, ALA434, LEU432, THR147; by alkyl interaction with LEU268, ILE253, TYR256, ILE143 and attractive charge interaction with ASP385. (E)-N-(2-amino-4-fluorophenyl)-3-(1-cinnamyl-1H-1,2,3-triazol-4-yl)acrylamide interacted with 7AIT by alkyl interactions with MET 436, LEU 333, ILE 439, TYR 442, TRP 84; by Pi-Pi T shaped interactions with TYR 334, PHE 330; by carbon hydrogen interactions with SER 81, SER 286; and van der Waal interactions with ASP 72, TYR 121, ASP 285, LEU 282, GLY 335. (E)-N-(2-amino-4-fluorophenyl)-3-(1-cinnamyl-1H-1,2,3-triazol-4-yl)acrylamide interacted with 6QAE by van der waal interactions with TYR128, GLU197, GLY439, GLY116, ILE442, SER287, GLN119, GLN119, THR120, PRO285, PHE329, ALA328, MET437, TYR440, TRP430, GLY115; by alkyl interactions with TRP82, HIS438; by pi-pi stacking interaction with TYR 332; halogen interaction with GLU 276 and hydrogen bond interactions with ASN68, ASN289. In a similar manner (E)-N-(2-amino-4-fluorophenyl)-3-(1-cinnamyl-1H-1,2,3-triazol-4-yl)acrylamide interacted with 3GB2 by van der waal interactions with ASP133, ILE62, VAL70, TYR134, THR138, GLN185, LYS183, ASN186, PHE67, SER203, SER66; by alkyl interactions with LEU188, VAL110, LEU132, CYS199, ALA83; by attractive charges with ASP200, ASP181; halogen interaction with GLY202 [20] (Figure 3).

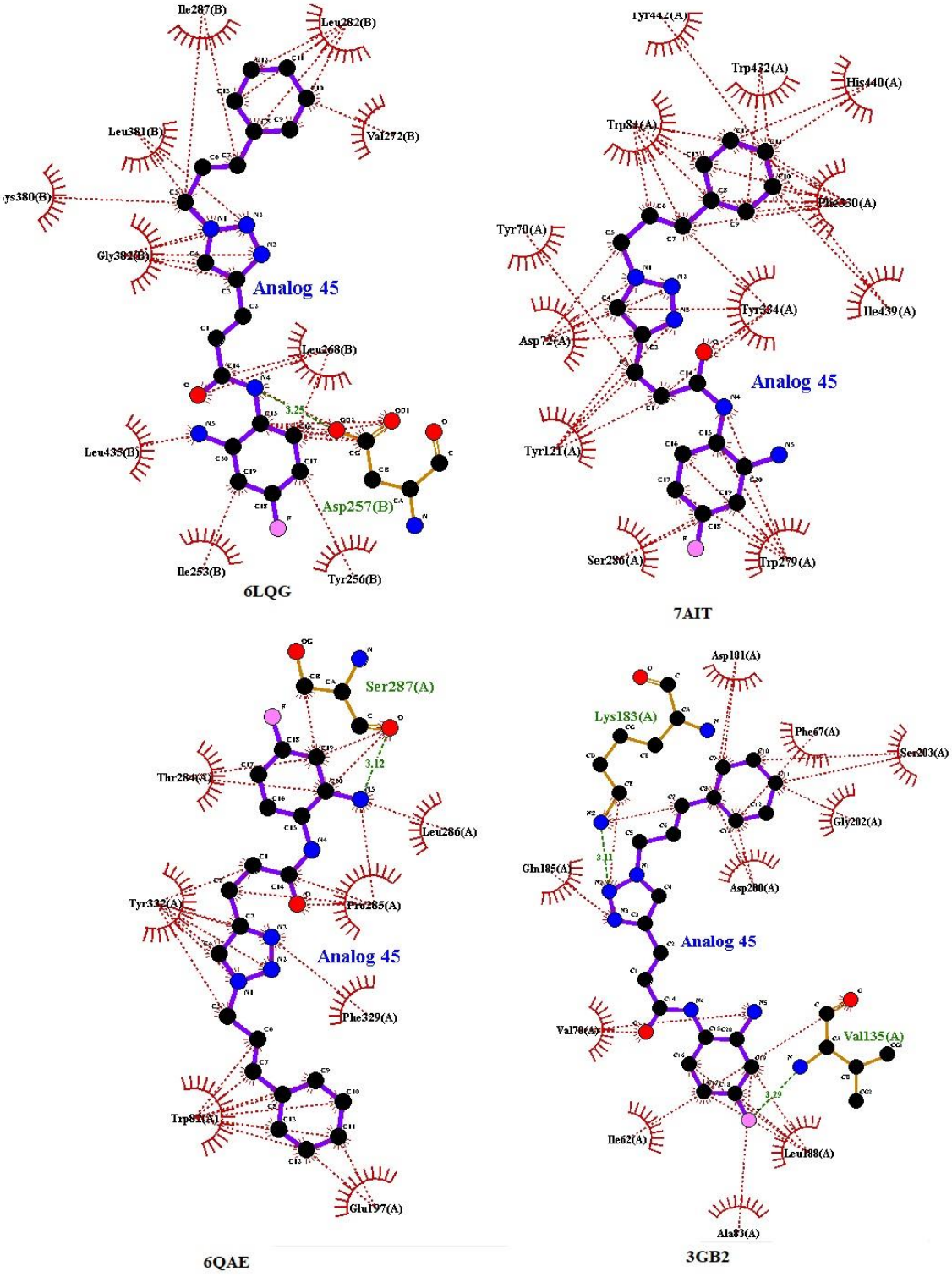

Figure 3. Molecular docking interactions between Analog 45 and 6LQG, 7AIT, 6QAE, 3GB2 receptors.

As per the interaction study data, N-methyl-4-((3-(pyrrolidin-1-ylmethyl)-1H-indol-1-yl)methyl)benzamide and 6LQG interacted with GLY384, PHE388, SER169, LEU173, ALA285, PHE237, SER170, LEU166, GLY382 via van der waal interactions; LEU286, LEU383, LEU226, ILE229, ILE213 via alkyl interactions; and with ILE387 via Pi-sigma interaction. N-methyl-4-((3-(pyrrolidin-1-ylmethyl)-1H-indol-1-yl)methyl)benzamide and 7AIT interacted with ILE439, TYR442, GLY119, PHE200, PHE119, GLY118, TYR121, SER122, TYR334, SER81, TRP432 via van der waal interactions; with HIS440 and TYR70 using alkyl interactions; and with PHE330 and TRP84 using Pi-Pi stacked interactions. N-

methyl-4-((3-(pyrrolidin-1-ylmethyl)-1H-indol-1-yl)methyl)benzamide and 6QAE interacted with TRP82 via conventional interaction; with THR120, TYR440, ALA328, GLN119, ASP70, TYR332, SER79, SER198, PHE398, GLY117, and VAL288 via van der waal interactions; with PHE329, TRP231 via Pi-Pi T shaped interaction; and TRP430 and LEU286 using alkyl interactions. N-methyl-4-((3-(pyrrolidin-1-ylmethyl)-1H-indol-1-yl)methyl)benzamide and 3GB2 interacted with ILE62, VAL70, LEU188, VAL110, LEU132, ALA83 via alkyl interactions; and with CYS199 using Pi-sulfur interaction (Figure 4).

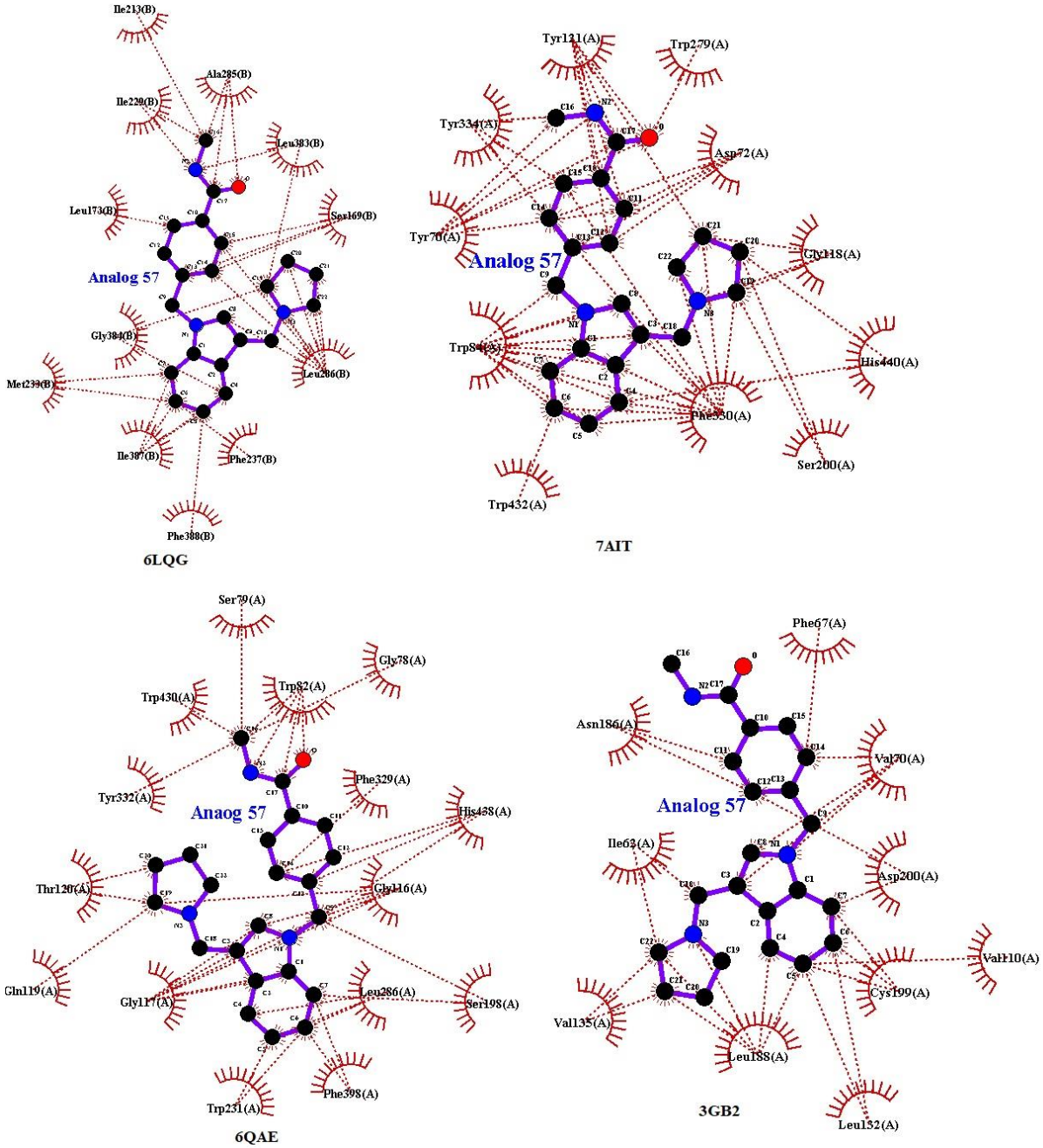

Figure 4 Molecular docking interactions between Analog 57 and 6LQG, 7AIT, 6QAE, 3GB2 receptors.

Molecular docking interaction data showed that (E)-N-(2-amino-4-fluorophenyl)-3-(1-cinnamyl-1H-1,2,3-triazol-4-yl)acrylamide, N-methyl-4-((3-(pyrrolidin-1-ylmethyl)-1H-indol-1-yl)methyl)benzamide and complexed ligand of 6LQG shared GLY382, and LEU268 as common amino acid residues. (E)-N-(2-amino-4-fluorophenyl)-3-(1-cinnamyl-1H-1,2,3-triazol-4-yl)acrylamide, N-methyl-4-((3-(pyrrolidin-1-ylmethyl)-1H-indol-1-yl)methyl)benzamide and complexed ligand of 7AIT shared TRP 84, and PHE 330 as common

amino acid residues. (E)-N-(2-amino-4-fluorophenyl)-3-(1-cinnamyl-1H-1,2,3-triazol-4-yl)acrylamide, N-methyl-4-((3-(pyrrolidin-1-ylmethyl)-1H-indol-1-yl)methyl)benzamide and co-crystallized ligand of 6QAE shared ALA328, TRP82 and TYR 332 as common amino acid residues. (E)-N-(2-amino-4-fluorophenyl)-3-(1-cinnamyl-1H-1,2,3-triazol-4-yl)acrylamide, N-methyl-4-((3-(pyrrolidin-1-ylmethyl)-1H-indol-1-yl)methyl)benzamide and complexed ligand of 3GB2 shared these ILE 62, VAL 70, and ALA 83 as common amino acid residues (Table 4). These common acid residues confirmed that (E)-N-(2-amino-4-fluorophenyl)-3-(1-cinnamyl-1H-1,2,3-triazol-4-yl)acrylamide (Analog 45) and N-methyl-4-((3-(pyrrolidin-1-ylmethyl)-1H-indol-1-yl)methyl)benzamide (Analog 57) successfully docked within the active site of the selected Alzheimer receptors. Finally, the molecular docking interaction study data confirmed that analog 57 showed maximum docking interactions against gamma-secretase, acetylcholinesterase, butyrylcholinesterase, and glycogen synthase kinase-3 beta enzymes, so this molecule was considered for further experiments.

Table 4. Interacting residues of the selected HDAC inhibitors and Rivastigmine docked against 6LQG, 7AIT, 6QAE, and 3GB2.

SN	Name of the Molecules	Amino acid residue 6LQG	Amino acid residue 7AIT	Amino acid residue 6QAE	Amino acid residue 3GB2
1	Rivastigmine (standard)	VAL272, ILE287, VAL261, GLY384, ALA434, ASP385, ASP257, GLY382 shows van der waals interaction, LEU268, LEU282 shows Pi-sigma interaction, PRO433, LEU271, LEU286, PHE283 shows alkyl interaction	GLY118, SER200, HIS440, ASP72, SER122, VAL71, TYR442 shows van der waal interaction, GLU199, ASN85 TYR121 shows carbon hydrogen bond, TRP84, PHE330 Pi-Pi stacked interaction, TYR70 shows alkyl interaction	SER198, HIS438 shows conventional hydrogen bond, GLY116 shows carbon hydrogen bond, MET437, TYR440, TRP430, ALA199, LEU286, GLY117 shows van der waal interaction.	LEU188, ILE62, VAL70, ALA83 shows carbon hydrogen interaction and GLN185 shows Pi alkyl interaction
2	Trichostatin A	ASP385, ASP257 shows conventional hydrogen bond, VAL261, GLY382, LEU268, LEU27, THR147, PRO433, ALA434, LEU435 shows van der waal interaction, TRP165, ILE143, MET146, LEU150, LEU286, LEU282, PHE283, ILE287 shows alkyl interaction	TYR70, SER81, ASP72, TY334, SER122, GLY118, SER200, TYR130, GLY117 shows van der waal interaction, GLU199 shows carbon hydrogen bond interaction, HIS440, TYR121 shows alkyl interaction, TRP84, PHE330 shows Pi-Pi stacked	TYR128, TYR332, GLU197 shows conventional hydrogen bond, THR120, SER79, TRP82 shows carbon hydrogen bond, GLY78, ILE442, TYR114, GLY115, SER198, GLY121, GLY116, LEU125, MET437 shows van der waal interaction	ASN186, LYS183 shows conventional hydrogen bond, VAL70 shows Pi alkyl bond and ILE62 shows carbon hydrogen bond
3	Tinostamustine	TYR389, LEU435, ILE387, ASP385, PHE389, LEU383, GLY382 shows van der waal interaction, PHE388 show conventional hydrogen bond	HIS440, PHE330, SER122, TYR334, TRP84, ASN85, ASP72, TRY70 shows the interaction	TRP82, HIS438, SER198, ALA199, ALA328, THR120, GLY117 shows the interaction	VAL110, CYS199, ALA83, LEU188, LEU132, TYR134, VAL70, PHE67 shows alkyl interaction, VAL135, ILE62, GLY63, ASN64, GLY65, ASP133, LYS183, ASP200, ASP181, UNL1, LYS85, ALA204 shows van der waals interaction, SER203, GLY202 shows conventional hydrogen bond
4	Panobinostat	ASP385, ASP257, LEU435 shows conventional interaction, PRO433, ASP257, ILE23, ILE143,	ARG289, SER286 shows conventional hydrogen bond, LEU282, PHE288,	GLY78, TRP430 shows conventional hydrogen bond,	ASP181, ASP200 shows conventional hydrogen bonding, ILE62, TYR134, LEU188, ALA83, LYS85,

SN	Name of the Molecules	Amino acid residue 6LQG	Amino acid residue 7AIT	Amino acid residue 6QAE	Amino acid residue 3GB2
		GLY384, PHE388, THR147 shows van der waal interaction, LEU150, LEU268,shows alkyl interaction, TYR256 shows Pi-Pi T shaped interaction	PHE290, SER122, GLY335, TYR70, SER81, TRP432, ILE439, TYR442, HOS440, SER122 shows van der waal interaction, ILE287, ASP72 shows carbon hydrogen bond, TYR121, TYR334, TRP279, TRP84, PHE330 shows alkyl interaction	GLY116, TYR332, PHE329, TRP231 shows Pi-Pi stacked, GLY439, ALA328, HIS438, SER198, PHE398, VAL288, ASP70, MET437, TRP82, SER79, TYR440, GLY117 shows van der waal interaction	CYS199 shows alkyl bonding
5	Pracinostat	LYS380 shows conventional hydrogen bond, ILE287, LEU282, GLY382, LEU381, LEU85, VAL379, LEU425, THR421, LEU432, PRO433, TYR256, GLY384, LEU268 shows van der waal interaction, LEU286, PHE283, ILE253, PHE388, LEU435, ALA434 shows alkyl interaction, ASP385 shows Pi- anion interaction	TRP432 sows Pi sigma interaction, MET436, ILE439 shows alkyl interaction, TRP84, GLN69, TYR70, ASP72 shows conventional hydrogen bond, HIS440, VAL71 shows carbon hydrogen bond, TYR334, TYR442, LEU333, TYR130,GLY199, SER200, GLY118, PHE331, TYR121, SER122, ASN85, PRO86, GLY123 shows van der waal interaction.	SER198, SER287, VAL288, TRP82, TYR332, THR120, ALA277,GLN119 shows van der waal interaction, GLY117 shows carbon hydrogen bond, TRP231, PHE329 shows Pi sigma interaction, GLU276, ASN68, ASN289 shows conventional hydrogen bond, PHE398, LEU286, HIS438, ALA328 shows alkyl interaction.	VAL110, ALA83, LEU188 LEU132 shows alkyl bonding, CYS199, ASP181, ASP200 shows conventional hydrogen bond and VAL70 shows Pi sigma bond
6	Abexinostat	PRO436, ASP385, GLY382, ILE287, PHE283, LEU282, THR147, LEU150, GLY384, LEU435, PRO433, LEU432 shows van der waal interaction, ALA434, ASP257, shows conventional hydrogen bond, ILE253, LEU268 shows alkyl interaction.	ARG289, PHE288 shows conventional hydrogen bond, PHE330, RP84, TYR334 shows Pi-Pi stacked interaction, SER286, PHE290, TRP279, TYR70, ASP72, ASN85, SER200, GLY118, HIS440, SER122, ILE439, TYR442, TRP432, PHE331, ILE287 shows van der waal interaction	TRP82, GLY116, SER198, HIS438, ASN68, ASP70 show conventional hydrogen bond, PRO84, THR120, GLY117, PHE398, VAL288 shows carbon hydrogen bond, GLY121, ASN83, GLN67, ILE69, THR120, GLY117, PHE398, VAL288, GLY117, GLU197, GLY115, GLY439 show van der waal interaction	ASP181, ASP200, ASN186 shows coventional hydrogen bond, GLY63 shows carbon hydrogen bond LEU188, ALA83, VAL70 shows Pi alkyl interaction
7	CXD101	LEU381 shows amide Pi stacked, ILE287, ILE253 shows alkyl interaction, GLU280 shows carbon hydrogen bond, LYS380, GLY382, LEU278, LEU268, LEU435, GLY384, PHE388, ASP385, TYR256, ALA275, THR281, PHE283 shows van der waal interaction	PHE330, TRP84, TYR334 shows Pi-sigma interaction, SER286 shows conventional hydrogen bond, TRP279, TYR70 shows alkyl interaction, GLY118, SER122, ASP72, TYR121, GLY335, ILE287, PHE288, ARG289, LEU282 shows van der waal interaction	GLY115 show carbon hydrogen bond, TYR332 show conventional hydrogen bond, GLY283 show Pi-Pi stacked, HIS438 show alkyl interaction, TRP82 shoe Pi- sigma interaction, GLU197, GLY439, TYR128, GLY121, GLY116, THR120, SER287, ALA277, PHE329GLY333 show van der waal interaction	VAL135, ASP200, ASP181 shows conventional hydrogen bond, ILE62, TYR134 shows alkyl interaction

SN	Name of the Molecules	Amino acid residue 6LQG	Amino acid residue 7AIT	Amino acid residue 6QAE	Amino acid residue 3GB2
8	Analog 34	ILE287, PHE283, LEU150, LEU271, LEU383, GLY382, ALA434, THR147, LEU435 shows van der waal interaction, ASP257, ASP385, GLY384 shows conventional hydrogen bond, LEU282, LEU286, TYR256, LEU268, ILE143, ILE253, PHE388 shows alkyl interaction	TYR130, LEU127, TYR116 shows alkyl interaction, TYR121 shows conventional hydrogen bond, TRP84, PHE330, GLY117 shows Pi-Pi stacked, SER124, GLY123, ASP72, HIS440, ILE439, TYR442, TRP432, TYR334, GLY80, SER200, GLU199, GY118, SER122 shows van der waal interaction	HIS438, ALA328, MET437, TRP430, TYR440, LEU286 show alkyl interaction, PHE329, TRP231 show Pi-Pi T shaped, TRP82 show Pi-sigma interaction, VAL288, GLY117, PHE398, SER198, GLU197, THR120, GLY117, GLY116, GLY439, ILE442 show van der waal interaction.	ALA83, LEU188 shows alkyl interaction, ASN186 shows conventional interaction and PHE67 shows Pi-Pi T shaped interaction
9	Analog 35	LEU432 shows conventional hydrogen bond, ALA434, LEU425, LEU381, LEU422 shows alkyl interaction, THR421, LYS380, LEU85, VAL379, ALA431 shows van der waal interaction	HIS440, ILE439, SER81 shows van der waal interaction, PHE330, TRP84, TRP432, TYR442 show Pi alkyl interaction, TYR334 shows conventional hydrogen bond	LEU286, TRP231, PHE329 show alkyl interaction, PHE398, GLY117, SER198, GLY116, GLU197, ALA199, GLY115 show van der waal interaction	VAL110, ALA83, CYS199, LEU188, LEU132, VAL70 shows alkyl interaction and ASP200 shows carbon hydrogen and alkyl interaction
10	Analog 36	ASP257, LEU435, ASP385, GLY384 with interaction	PHE330, TRP84 show alkyl interaction	TRP82, GLY116, HIS438, LEU286, PHE398, LEU286, ALA328, PHE329, show interaction	VAL135, PRO136, VAL110, ASP200, ASP133, LYS85, LEU132, CYS199 shows van der waals interaction, TYR134, ALA83, LEU188, ILE62, VAL70, PHE67 Shows alkyl interaction
11	Analog 39	ALA431, VAL272, VAL261, LEU425, LEU381, LEU435, PHE388 show alkyl interaction, ASP385, ALA34 show conventional hydrogen bond, LYS380, LEU432, LEU268, THR421 show van der waal interaction	VAL71, SER81, PHE330, PHE290, PHE288, ILE287, SER286, GLY335 shows van der waal interaction, TRP 84, ASN85 show halogen, TYR121, TRP279 show Pi-Pi T shaped interaction TYR70 alkyl interaction	GLN71 shows conventional hydrogen bond, GLY116, ASP70 show carbon hydrogen bond, ASN68, THR120, PHE329, GLY115, GLY121, TYR128, ILE442, GLU197, GLY439, ALA328, HIS438, SER79, TYR332 show van der waal interaction	ILE62, LEU188, ALA83, LEU132, VAL110, CYS199, VAL70 shows alkyl interaction, VAL135, TYR134, ASP133, LYS183, ASN186, ASP200, PHE67, SER66, GLN185, GLY63, THR138 shows van der waals interaction
12	Analog 45	LEU282 shows Pi sigma interaction, ASP257, LEU271, LEU150, PHE283, LEU286, ILE287, GLY382, LEU381, LYS380, THR421, LEU422, LEU425, ALA434, LEU432, THR147 shows van der waal interaction LEU268, ILE253, TYR256, ILE143 shows alkyl interaction, ASP385 shows attractive charge	MET436, LEU333, ILE439, TYR442, TRP84 shows alkyl interaction, TYR334, PHE330 shows Pi-Pi T shaped interaction, SER81, SER286 shows carbon hydrogen bond, ASP72, TYR121, ASP285, LEU282, GLY335 shows van der waal interaction.	TYR128, GLU197, GLY439, GLY116, ILE442, SER287, GLN119, GLN119, THR120, PRO285, PHE329, ALA328, MET437, TYR440, TRP430, GLY115 show van der waal interaction, TRP82, HIS438 show alkyl interaction TYR332 show Pi-Pi stacked, GLU276 show halogen, ASN68, ASN289 show	ASP133, ILE62, VAL70, TYR134, THR138, GLN185, LYS183, ASN186, PHE67, SER203, SER66 shows van der Waals interaction, LEU188, VAL110, LEU132, CYS199, ALA83 shows alkyl interaction, ASP200, ASP181 shows attractive charges, GLY202 shows halogen (fluorine) interaction

SN	Name of the Molecules	Amino acid residue 6LQG	Amino acid residue 7AIT	Amino acid residue 6QAE	Amino acid residue 3GB2
				conventional hydrogen bond.	
13	Analog 47	ILE387, LEU286, LEU282, ILE287, PHE283, LEU432, LEU425, LEU381, GLY382 shows van der interaction, LEU269, VAL272, VAL261, ALA431 shows Pi alkyl interaction, LYS380 show carbon hydrogen bond	TRP432, TYR70 shows carbon hydrogen bond, PHE330, TRP84 shows Pi-Pi stacked , LEU333, HIS440, TYR334, MET436, ILE439, TYR442, SER81, ASP72, ASN85, GLN69, VAL71, PRO86, SER122, GLY123, GLY118, GLY117, LEU127, TYR130, HIS440 shows van der waal interaction	GLU276, LEU273, ALA277, ASN68, THR120, ASN83, TRP82, GLY116, HIS438, SER198, PHE329, GLY117 show van der waal interaction, ASN289, GLN119 show conventional hydrogen bond	ILE62, VAL70 shows alkyl interaction and GLY65, ASP133 shows carbon hydrogen bond interaction
14	Analog 48	THR147, ILE143, TYR256, ILE253, PRO433, ASP385, LEU432, LYS380, LEU381, GLY382 shows van der waal interaction, ALA434 shows conventional hydrogen bond, LEU150, LEU268 shows alkyl interaction, ASP257 shows Pi anion interaction	TYR334, TRP279 shows Pi-Pi stacked, PRO86 show alkyl interaction, VAL71, GLN69, ASN85, SER81, PHE330, ILE287, SER286, GLY123, SER122, TYR70, ASP72, TYR121 shows van der waal interaction, GLY335 shows carbon hydrogen bond.	ILE442, GLU197, GLY439, TYR440, MET437, TRP430, PHE329, PRO285, ASP70 show van der waal interaction, ALA328 show alkyl interaction, TRP82 show Pi sigma, TYR332 show Pi-Pi T shaped interaction	ALA83, CYS199, TYR134, LEU188, ILE62, LYS85 shows alkyl interaction, VAL70 shows Pi sigma interaction, PHE67 shows Pi-Pi T shaped interaction and GLY65 shows carbon hydrogen bond interaction
15	Analog 49	VAL272, ALA275, GLU280, THR281, LYS380, GLY382, ALA434, PRO433, VAL261, ASP257 shows van der waal interaction, LEU282 shows Pi sigma interaction, ILE287, LEU268 shows alkyl interaction.	TRP84, PHE330, TYR334 shows Pi-Pi stacked, TRP 279 show Pi donor hydrogen bond, TYR442, ILE439, TRP432, SER81, TYR121, TYR70 shows van der waal interaction.	PHE398, SER198, TYR332, SER79, ALA328, MET437, GLY117, PRO285, SR287, VAL288 show van der waal interaction, TRP82, TRP430, TYR440, GLY78 show conventional hydrogen bond, LEU286 show alkyl interaction	VAL70, ALA83, LYS85, LEU188 shows alkyl interaction, PHE67 shows Pi-Pi T shaped interaction and CYS199 and GLY65 shows Pi donor hydrogen bond interaction
16	Analog 51	VAL272, THR281, LEU432, THR421, LEU381, LEU425, TYR77, VAL379, GLY382, PRO433, LEU268, ASP257, ASP385 show van der waal interaction, LYS380 show conventional hydrogen bond, LEU282, ILE287, ALA434 shows Pi alkyl interaction	VAL71, TYR121, ASP72, SER81, TYR70, PRO86, SER122, ASN85, GLY118, GLY117, GLN69, GLU199, HIS440, TYR442, LEU333, TYR334, ILE444 show van der waal interaction, SER200 show conventional hydrogen bond, TRP432 show Pi sigma, ILE439, MET436 show alkyl interaction	ASP70 show conventional hydrogen bond, SER198, TYR440, TRP430, MET437, GLY78, ALA328, SER79, ASN83, GLY121, THR120, ILE69, GLY116, GLY117, VAL288, PHE398 show van der waal interaction	ASN186, GLY63, LYS183, PHE67, ASN64, GLY65, CYS199, VAL110, GLU97, PHE201, LEU132, LYS85, PRO136, VAL135 show van der waal interaction, VAL70, ILE62, LEU188, TYR134, ALA83 show alkyl interaction, ASP200 Pi anion interaction.
17	Analog 57	GLY384, PHE388, SER169, LEU173, ALA285, PHE237, SER170, LEU166, GLY382 show van der waal interaction, LEU286, LEU383, LEU226, ILE229, ILE213 show alkyl interaction, ILE387 show Pi-sigma interaction.	ILE439, TYR442, GLY119, PHE200, PHE119, GLY118, TYR121, SER122, TYR334, SER81, TRP432 show van der waal interaction, HIS440, TYR70 show alkyl interaction,	TRP82 show conventional interaction, THR120, TYR440, ALA328, GLN119, ASP70, TYR332, SER79, SER198, PHE398, GLY117, VAL288 show van	ILE62, VAL70, LEU188, VAL110, LEU132, ALA83 shows alkyl interaction and CYS199 shows Pi-sulfur interaction

SN	Name of the Molecules	Amino acid residue 6LQG	Amino acid residue 7AIT	Amino acid residue 6QAE	Amino acid residue 3GB2
			PHE330, TRP84 show Pi-Pi stacked interaction	der waal interaction, PHE329, TRP231 show Pi-Pi T shaped interaction, TRP430, LEU286 alkyl	

3.3. Osiris-molinspiration data.

As we know, if the bioactivity score was more than 0.00, then the molecule became active; if the bioactivity score was between -0.50 and 0.00, then the molecule became moderately active; and finally, if the score was less than -0.50, then the molecule became inactive. Keeping the above criteria in mind, we can say that Trichostatin-A, Tinostamustine, Panobinostat, Pracinostat, Analog 34, Analog 39, Analog 48, Analog 51, and Analog 57 may show biological activity through GPCR protein, going on the list only Analog 34 may work through ion channel modulation. Trichostatin-A, Tinostamustine, Pracinostat, CXD101, Analog 34, Analog 39, Analog 45, Analog 47, Analog 48, Analog 49, Analog 51, Analog 57 work through kinase pathway, Trichostatin-A, Analog 39, Analog 49, Analog 51 work through nuclear receptor ligand pathway. Trichostatin-A, Tinostamustine, Panobinostat, Pracinostat, Abexinostat, Analog 34, Analog 48, Analog 49, Analog 51, Analog 57 follow protease inhibitor pathway and lastly Trichostatin-A, Tinostamustine, Panobinostat, Pracinostat, Abexinostat, Analog 34, Analog 39, Analog 45, Analog 47, Analog 48, Analog 49, Analog 51 and Analog 57 follow enzyme inhibitor pathway. We have come to the conclusion that analog 57 shows results better than or near the standard (Rivastigmine) as it won't show mutagenicity, tumorigenicity, irritancy, or reproductive toxicity. Moreover, cLogP of analog 57 is 3.04, solubility is -2.8, molecular weight 347, TPSA 37.27, drug-likeness 2.08, and drug score is 0.78. At the same time, Rivastigmineshows cLogP, solubility, molecular weight, TPSA, drug-likeness, and drug score as 1.98, -1.62, 250, 32.78, 1.81, and 0.87, respectively (Figure 5) (Table 5) [22].

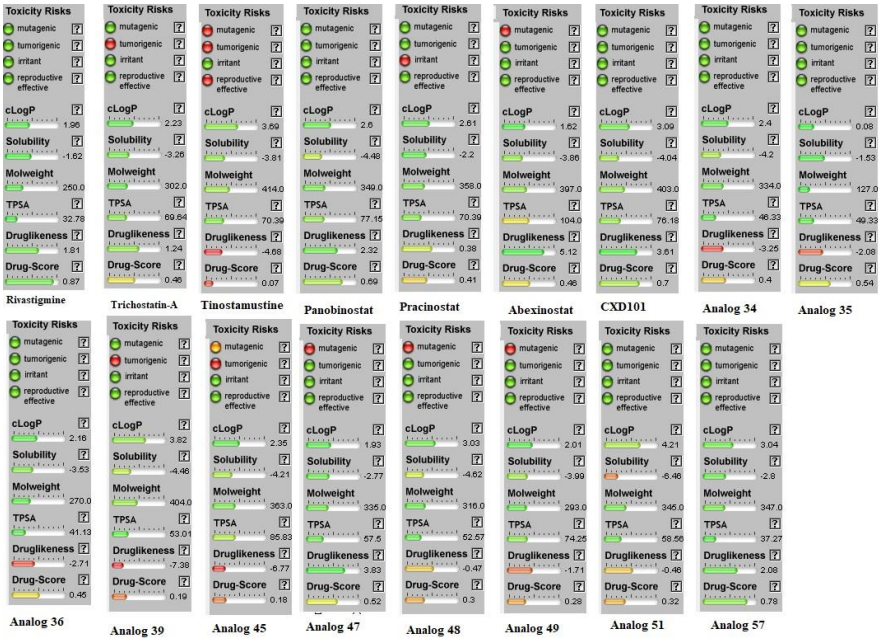

Figure 5. Osiris-Molinspiration data of the selected HDAC inhibitors and Rivastigmine.

Table 5. Molinspiration data of the selected HDAC inhibitors and Rivastigmine.

SN	Molecule Name	Activity type	Bioactivity Score
1.	Rivastigmine	GPCR ligand	-0.05
		Ion channel modulator	0.06
		Kinase inhibitor	-0.38
		Nuclear receptor ligand	-0.35
		Protease inhibitor	-0.18
		Enzyme inhibitor	-0.01
2.	Trichostatin-A	GPCR ligand	0.05
		Ion channel modulator	-0.17
		Kinase inhibitor	0.16
		Nuclear receptor ligand	0.38
		Protease inhibitor	0.22
		Enzyme inhibitor	0.63
3.	Tinostamustine	GPCR ligand	0.18
		Ion channel modulator	-0.27
		Kinase inhibitor	0.26
		Nuclear receptor ligand	-0.12
		Protease inhibitor	0.42
		Enzyme inhibitor	0.35
4.	Panobinostat	GPCR ligand	0.27
		Ion channel modulator	-0.11
		Kinase inhibitor	0.27
		Nuclear receptor ligand	-0.08
		Protease inhibitor	0.34
		Enzyme inhibitor	0.51
5.	Pracinostat	GPCR ligand	0.34
		Ion channel modulator	-0.19
		Kinase inhibitor	0.11
		Nuclear receptor ligand	-0.16
		Protease inhibitor	0.32
		Enzyme inhibitor	0.44
6.	Abexinostat	GPCR ligand	-0.01
		Ion channel modulator	-0.44
		Kinase inhibitor	-0.01
		Nuclear receptor ligand	-0.42
		Protease inhibitor	0.35
		Enzyme inhibitor	0.11
7.	CXD101	GPCR ligand	-0.02
		Ion channel modulator	-0.30
		Kinase inhibitor	0.07
		Nuclear receptor ligand	-0.67
		Protease inhibitor	-0.22
		Enzyme inhibitor	-0.11
8.	Analog 34	GPCR ligand	0.50
		Ion channel modulator	0.33
		Kinase inhibitor	0.28
		Nuclear receptor ligand	-0.18
		Protease inhibitor	0.63
		Enzyme inhibitor	0.20
9.	Analog 35	GPCR ligand	-1.76
		Ion channel modulator	-2.30
		Kinase inhibitor	-2.28
		Nuclear receptor ligand	-2.15
		Protease inhibitor	-0.74
		Enzyme inhibitor	-0.72
10.	Analog 36	GPCR ligand	-0.66
		Ion channel modulator	-0.74
		Kinase inhibitor	-0.71
		Nuclear receptor ligand	-1.29
		Protease inhibitor	-0.76
		Enzyme inhibitor	-0.39
11.	Analog 39	GPCR ligand	0.04
		Ion channel modulator	-0.04
		Kinase inhibitor	0.12
		Nuclear receptor ligand	0.14
		Protease inhibitor	-0.25

SN	Molecule Name	Activity type	Bioactivity Score
		Enzyme inhibitor	0.06
12.	Analog 45	GPCR ligand	-0.07
		Ion channel modulator	-0.34
		Kinase inhibitor	0.08
		Nuclear receptor ligand	-0.53
		Protease inhibitor	-0.09
		Enzyme inhibitor	0.16
13.	Analog 47	GPCR ligand	-0.07
		Ion channel modulator	-0.34
		Kinase inhibitor	0.08
		Nuclear receptor ligand	-0.53
		Protease inhibitor	-0.09
		Enzyme inhibitor	0.16
14.	Analog 48	GPCR ligand	0.14
		Ion channel modulator	-0.14
		Kinase inhibitor	0.24
		Nuclear receptor ligand	-0.08
		Protease inhibitor	0.47
		Enzyme inhibitor	0.42
15.	Analog 49	GPCR ligand	0.12
		Ion channel modulator	-0.13
		Kinase inhibitor	0.48
		Nuclear receptor ligand	-0.25
		Protease inhibitor	0.46
		Enzyme inhibitor	0.52
16.	Analog 51	GPCR ligand	0.18
		Ion channel modulator	-0.18
		Kinase inhibitor	0.32
		Nuclear receptor ligand	0.27
		Protease inhibitor	0.36
		Enzyme inhibitor	0.52
17.	Analog 57	GPCR ligand	0.35
		Ion channel modulator	-0.11
		Kinase inhibitor	0.23
		Nuclear receptor ligand	-0.16
		Protease inhibitor	0.18
		Enzyme inhibitor	0.15

3.4.FMO analysis data.

The chemical reactivity of a molecule directly depends upon its orbital energy. Inside a molecule, an electron flows from an electron-rich HOMO to an electron-deficient LUMO. HOMO orbital [Energy: (-) 5.53eV] reflected that the HOMO orbital localized on the indole nucleus, and LUMO orbital [Energy: (-) 1.24 eV] reflected that the orbital localized on N-methyl benzamide group. The energy gap between HOMO and LUMO orbitals correlated with the chemical reactivity and kinetic stability. Small energy gaps reflected more polarizability. High polarizability showed high chemical reactivity and low kinetic stability. High chemical reactivity and low kinetic stability are established as soft molecules. The molecule showed an energy gap of 4.29 eV, which confirmed the stable nature of N-methyl-4-((3-(pyrrolidin-1-ylmethyl)-1H-indol-1-yl)methyl)benzamide (Analog 57). This low energy gap value makes the molecule soft, which confirms that the molecule easily donates an electron to an acceptor molecule. The energy of the smaller band space gap increases the reactive nature and stability of the compound. In addition, the compound characterized based on reactivity, chemical hardness (η), electronegativity (μ), softness (ζ), and electrophilicity index (Ψ) were determined using the formulas:

Chemical hardness $\eta = \frac{I-A}{2}$;

Softness $\zeta = \frac{1}{2\eta}$; Electronegativity $\mu = -\frac{I+A}{2}$;

Electrophilicity index $\Psi = \frac{\mu^2}{\eta}$

where A and I is electron affinity and ionization potential, A = -E_{LUMO} and I = -E_{HOMO}.

Bond energy, dihedral energy, electrostatic energy, and the van der Waal energy of the molecule confirmed the electron density of the molecule(Figure 6) (Table 6) [23, 24].

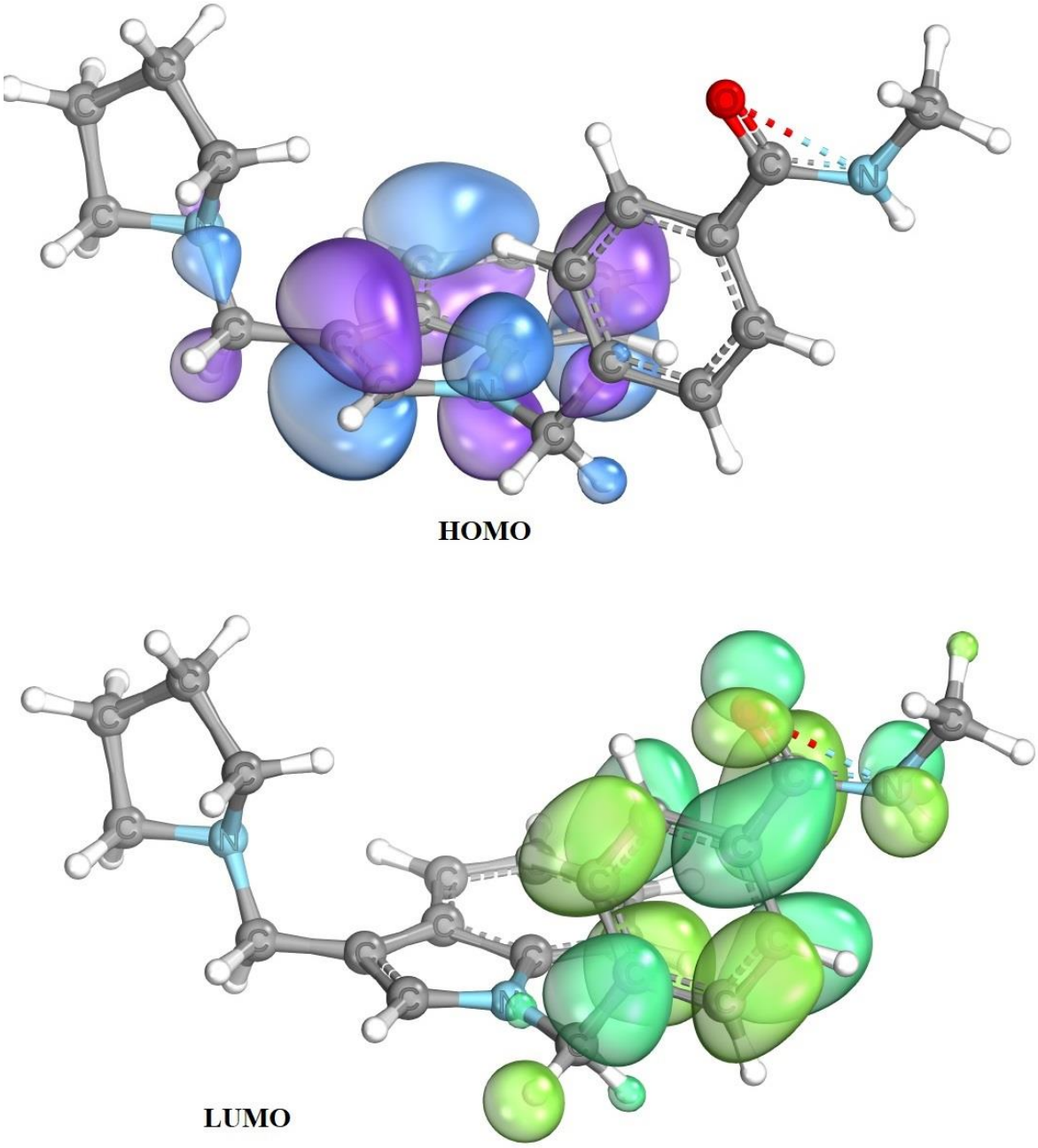

Figure 6 FMO analysis data of Analog 57.

Table 6. FMO analysis data of N-methyl-4-((3-(pyrrolidin-1-ylmethyl)-1H-indol-1-yl)methyl) benzamide (Analog 57).

E_{HOMO} (eV)	(-) 5.53
E_{LUMO} (eV)	(-) 1.24
ΔE gap (eV)	4.29
I	5.53

A	1.24
η	2.14
ζ	0.23
μ	3.38
Ψ	2.26
Bond energy	1.17272 kcal/mol
Angle Energy	95.93731 kcal/mol
Dihedral energy	6.46676 kcal/mol
Electrostatic energy	-19.21518 kcal/mol
Van der Waal energy	8.99357 kcal/mol

3.5. ESP investigation data.

The higher negative region was placed on the nitrogen atoms of pyrrolidine and indole [3-[(pyrrolidin-1-yl)methyl]-1*H*-indole of this nucleus], and also O=C-N of benzamide nucleus in red color were the most feasible position for electrophilic attack [25-27]. Similarly, benzene of indole ring and terminal methyl group of benzamide in blue color were the most suitable places for nucleophilic attack (Figure 7) [28, 29].

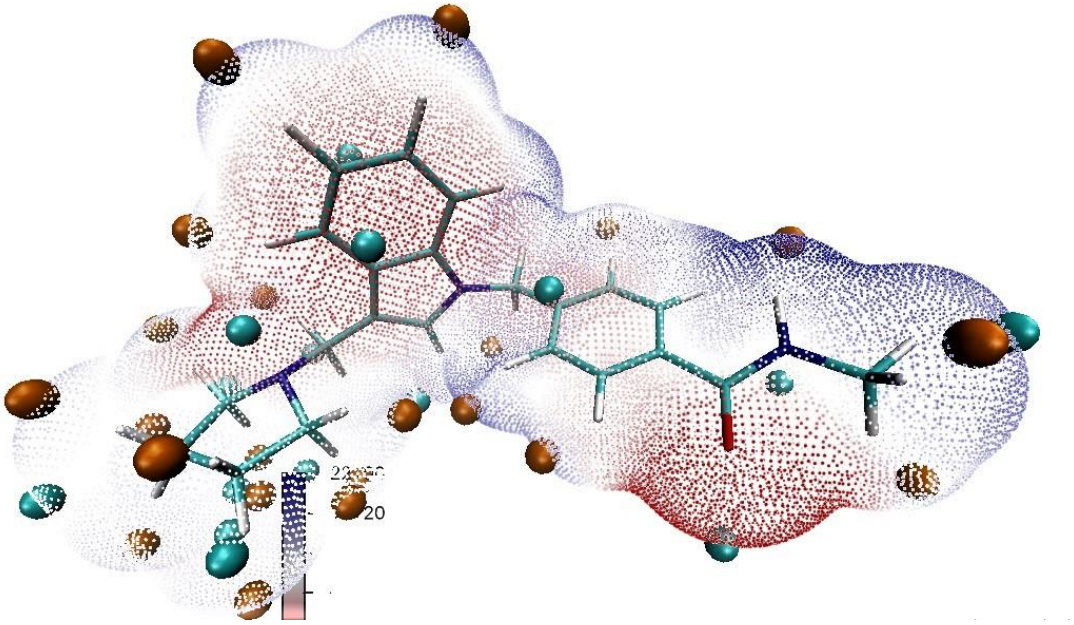

Figure 7 ESP analysis data of Analog 57.

4. Conclusions

After performing the computational studies using histone deactylase inhibitors targeting gamma-secretase, acetylcholinesterase, butrylcholinesterase, and glycogen synthase kinase enzymes in the treatment of Alzheimer disease, Analog 57 [N-methyl-4-((3-(pyrrolidin-1-ylmethyl)-1H-indol-1-yl)methyl) benzamide] showed good results in all aspect. So, it was concluded that among all the 60 HDAC inhibitors, Analog 57 is the best molecule. If we consider this molecule in the future, it may be a boon for humankind.

Funding

No funding from external or internal organizations.

Acknowledgments

Authors conveyed special thanks to Mr. Jitender Joshi, Chancellor, and Prof. (Dr.) Dharam Buddhi, Vice Chancellor of Uttaranchal University-Dehradun encourages publishing this research work. We are grateful to the Division of Research and Innovation (DRI) and Central Instrumentation Facility (CIF), Uttaranchal University-Dehradun, India, for providing all facilities during the experimental work.

Conflicts of Interest

No conflict of interest is associated with this work.

References

1. Hur, J.Y. γ-Secretase in Alzheimer's disease. *Exp. Mol. Med.***2022**, *54*, 433-446, https://doi.org/10.1038/s12276-022-00754-8.
2. Marucci, G.; Buccioni, M.; Ben, D.; Lambertucci, C.; Volpini, R.; Amenta, F. Efficacy of acetylcholinesterase inhibitors in Alzheimer's disease. *Neuropharmacol.***2021**, *190*, 108352, https://doi.org/10.1016/j.neuropharm.2020.108352.
3. Ho, T.C.; Chan, A.H.; Ganesan, A. Thirty years of HDAC inhibitors: 2020 insight and hindsight. *J. Med. Chem.***2020**, *63(21)*, 12460-124684, https://doi.org/10.1021/acs.jmedchem.0c00830.
4. Mehta, M.; Prasher, P.; Sharma, M.; Shastri, M.D.; Khurana, N.; Vyas, M.; Dureja, H.; Gupta, G.; Anand, K.; Satija, S.; Chellappan, D.K.; Dua, K. Advanced drug delivery systems can assist in targeting coronavirus disease (COVID-19): A hypothesis. *Medical. Hypotheses.***2020**, *144*, 110254, https://doi.org/10.1016/j.mehy.2020.110254.
5. Saha, S.; Pal, D. Role of Histone Deacetylase Inhibitors on Viral Replication: A Review.*Biointerface. Res. Appl. Chem.***2023**, *13*, 1-18, https://www.researchgate.net/profile/Supriyo-Saha-2/publication/370264307_Role_of_Histone_Deacetylase_Inhibitors_on_Viral_Replication_A_Review/links/6448afbdd749e4340e388c60/Role-of-Histone-Deacetylase-Inhibitors-on-Viral-Replication-A-Review.pdf.
6. Wang, J.; Ge, Y.; Xie, X.Q. Development and testing of drug like screening libraries. *J. Cheminform. Modeling.***2019**, *59*, 53-65, https://doi.org/10.1021/acs.jcim.8b00537.
7. Gleb, N.Z.; Larisa, A. M.; Larisa, Y. K.; Alexander, V. C. Inhibitors of Intracellular Signaling Molecules: New Horizons in Drug Discovery for the Treatment of Alzheimer's Disease. *Biointerface. Res. Appl. Chem.***2023**, *13*, 2-11, https://biointerfaceresearch.com/wp-content/uploads/2023/01/BRIAC135.401.pdf.
8. Fatemeh, M.; Majid, M. Aging Genome Modification and Editing using the Crispr-Cas9 system: Anti-Alzheimer Study by Docking Methods. *Biointerface. Res. Appl. Chem.***2023**, *13*, 1-23, https://doi.org/10.33263/BRIAC133.224.
9. Daina, A.; Michielin, O.; Zoete, V. SwissADME: a free web tool to evaluate pharmacokinetics, drug-likeness and medicinal chemistry friendliness of small molecules. *Sci. Rep.***2017**, *7*, 42717, https://doi.org/10.1038/srep42717.
10. Hosen, M.I.; Mukhrish, Y.E.; Jawhari, A.H.; Celik, I.; Erol, M.; Abdallah, E.M.; Al-Ghorbani, M.; Baashen, M.; Almalki, F.A.; Laaroussi, H.; Hadda, T.B.; Kawsar, S.M.A. Design, Synthesis, In Silico and POM Studies for the Identification of the Pharmacophore Sites of Benzylidene Derivatives. *Molecules.***2023**; *28*, 2613, https://doi.org/10.3390/molecules28062613.
11. Marshall, S.A.; Payne, K.A.P.; Fisher, K.; White, M.D.; Ni Cheallaigh, A.; Balaikaite, A.; Rigby, S.E.J.; Leys, D. The UbiX flavin prenyltransferase reaction mechanism resembles class I terpene cyclase chemistry. *Nat. Commun.***2019**, *10*, 2357, https://doi.org/10.1038/s41467-019-10220-1
12. Viayna, E.; Coquelle, N.; Cieslikiewicz-Bouet, M.; Cisternas, P.; Oliva, C.A.; Sanchez-Lopez, E.; Ettcheto, M.; Bartolini, M.; De Simone, A.; Ricchini, M.; et al. Discovery of a Potent Dual Inhibitor of Acetylcholinesterase and Butyrylcholinesterase with Antioxidant Activity that Alleviates Alzheimer-like Pathology in Old APP/PS1 Mice. *J. Med. Chem.***2021**, *64*, 812-839, https://doi.org/10.1021/acs.jmedchem.0c01775.

13. Meden, A.; Knez, D.; Jukic, M.; Brazzolotto, X.; Grsic, M.; Pislar, A.; Zahirovic, A.; Kos, J.; Nachon, F.; Svete, J.; Gobec, S.; et. al. Tryptophan-derived butyrylcholinesterase inhibitors as promising leads against Alzheimer's disease. *Chem. Commun. (Camb).***2019**, *55*, 3765-3768, https://doi.org/10.1039/c9cc01330j.
14. Saitoh, M.; Kunitomo, J.; Kimura, E.; Iwashita, H.; Uno, Y.; Onishi, T.; Uchiyama, N.; Kawamoto, T.; Tanaka, T.; Mol, C.D.; et al. 2-{3-[4-(Alkylsulfinyl)phenyl]-1-benzofuran-5-yl}-5-methyl-1,3,4-oxadiazole derivatives as novel inhibitors of glycogen synthase kinase-3beta with good brain permeability. *J Med Chem.***2009**, *52*, 6270-6286, https://doi.org/10.1021/jm900647e.
15. Krishnan, V.; Verma, P.; Saha, S.; Singh, B.; Vinutha, T.; Kumar, R.R.; Kulshreshta, A.; Singh, S.P.; Sathyavathi, T.; Sachdev, A.; Praveen, S. Polyphenol-enriched extract from pearl millet (Pennisetumglaucum) inhibits key enzymes involved in post prandial hyper glycemia (α-amylase, α-glucosidase) and regulates hepatic glucose uptake. *Biocatalysis. Agricultural. Biotechnology.***2022**, *43*, 102411, https://doi.org/10.1016/j.bcab.2022.102411.
16. Kushwaha, P.P.; Singh, A.K.; Bansal, T.; Yadav, A.; Prajapati, K.S.; Mohd, S.; Kumar, S. Identification of Natural Inhibitors Against SARS-CoV-2 Drugable Targets Using Molecular Docking, Molecular Dynamics Simulation, and MM-PBSA Approach. *Frontiers. Cellular. Infection. Microbiol.***2021**, *11*, Article 730288, https://doi.org/10.3389/fcimb.2021.730288.
17. Fatonah, A.; Tambunan, U.S.F.; Pamungkas, W.O.; Dewanto, G. L.; Wicaksono, I.S. Discovery of GPX4 inhibitor by molecular docking simulation as a potential ferroptosis inducer. *Biointerface. Res. Appl. Chem.* **2020**, *10*, 4929 -4933, https://doi.org/10.33263/BRIAC101.929933.
18. Joshi, B.C.; Juyal, V.; Sah, A.N.; Saha, S. Computational Investigation of Geniposidic Acid as an Anticancer Agent Using Molecular Docking, Molecular Dynamic Simulation, DFT Calculation, and OSIRIS-Molinspiration Profiling. *Phys. Chem. Res.***2023**, *11*, 801-823, https://www.physchemres.org/article_163067.html.
19. Galvelis, R.; Doerr, S.; Damas, J.M.; Harvey, M.J.; De Fabritiis, G. A scalable molecular force field parameterization method based on density functional theory and quantum-level machine learning. *J. Chem. Inform. Modeling.***2019**, *59*, 3485-3493, https://doi.org/10.1021/acs.jcim.9b00439.
20. Bannwarth, C.; Caldeweyher, E.; Ehlert, S.; Hansen, A.; Pracht, P.; Seibert, J.; Spicher, S.; Grimme, S. Extended tight-binding quantum chemistry methods. Wiley Interdisciplinary Reviews: *Computational. Molecular. Sci.***2021**, *11*, e1493, https://doi.org/10.1002/wcms.1493.
21. Devereux, C.; Smith, J.S.; Huddleston, K.K.; Barros, K.; Zubatyuk, R.; Isayev, O.; Roitberg, AE. Extending the applicability of the ANI deep learning molecular potential to sulfur and halogens. *J. Chemical. Theor. Computation.***2020**, *16*, 4192-202, https://doi.org/10.1021/acs.jctc.0c00121.
22. Saha, S.; Pal, D.; Kumar, S. Design, synthesis and antiproliferative activity of hydroxyacetamide derivatives against HeLa cervical carcinoma cell and breast cancer cell line. Tropical. *J. Pharmaceut. Res. **2016**, 15*, 1319-26; https://doi.org/10.4314/tjpr.v15i7.8.
23. Saha, S, Pal, D.; Nimse, S.B. Recent Advances in the Discovery of GSK-3 Inhibitors from Synthetic Origin in the Treatment of Neurological Disorders. *Current. Drug. Target.***2021**. *22*, 1437-1461, https://doi.org/10.2174/1389450122666210120143953.
24. Saha, S.; Yeom, G.S.; Nimse, S.B.; Pal, D. Combination Therapy of Ledipasvir and Itraconazole in the Treatment of COVID-19 Patients Coinfected with Black Fungus: An In Silico Statement. *Biomed. Res. Int.* Article ID 5904261, **2022**, https://doi.org/10.1155/2022/5904261.
25. Saha, S.; Pal, D. 2D QSAR approach to develop newer generation small molecules active against SARS-COVID. *Int. J. Pharm. Sci. Res.***2023**, *14*, 1372-1391, https://doi.org/10.13040/IJPSR.0975-8232.14(3).1372-91.
26. Kerru, N.; Gummidi, L.; Bhaskaruni, S.V.H.S.; Maddila, S.N.; Singh, P.; Jonnalagadda, S.B. A comparison between observed and DFT calculations on structure of 5-(4-chlorophenyl)-2-amino-1,3,4-thiadiazole. *Sci. Rep.***2019**, *9*, 19280,https://doi.org/10.1038/s41598-019-55793-5.
27. Boutaina, A.; Bouchra, E. K.; Souraya, S.; Reda, D.; Abdelhakim, E.; Abdelaziz, S. Synthesis and Molecular Docking Studies of some Pyrano[2,3-c] Pyrazole as an Inhibitor of SARSCoronavirus 3CL Protease. *Lett. Appl. NanoBioSci.***2022**, *11*, 3780-81. https://doi.org/10.33263/LIANBS113.37803801.
28. Pelin, K.; Rebaz, A.O.DFT Calculation for Newly Synthesized 2-Chloro-1-(3- methyl-3-mesityl-cyclobutyl)-ethanone. *Lett. Appl. NanoBioSci.***2023**, *12*, 1-13. https://doi.org/10.33263/LIANBS124.114.
29. Oluwatoba, E.O. DFT and Monte Carlo Simulations on the Corrosion Inhibitive Potentials of some Furan-based Carbohydrazide Derivatives. *Lett. Appl. NanoBioSci.***2023**, *12*, 113. https://doi.org/10.33263/LIANBS124.113.